Article

Current Biology

Orbitofrontal cortex modulates auditory cortical sensitivity and sound perception in Mongolian gerbils

Graphical abstract

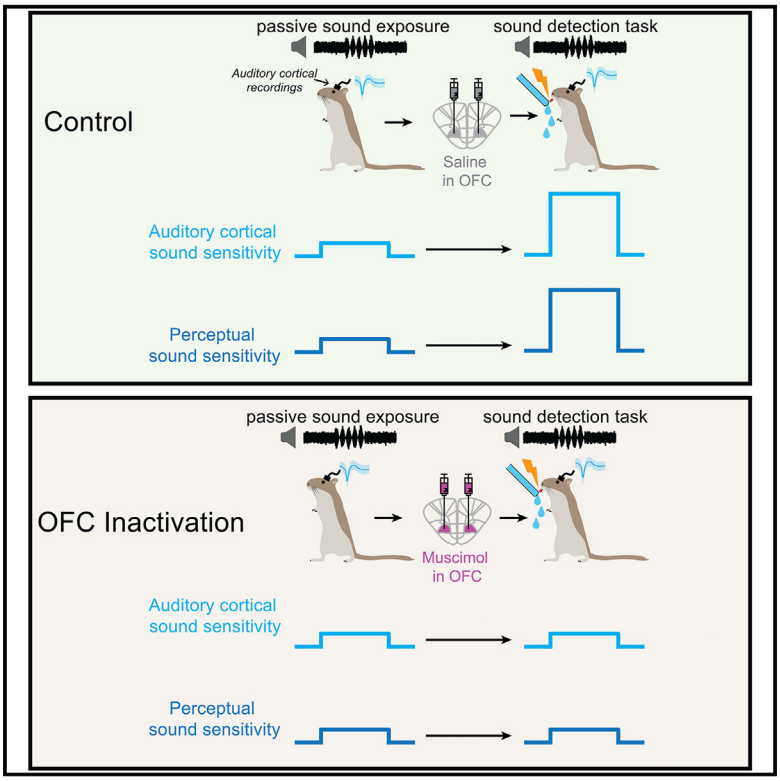

Authors

Matheus Macedo-Lima, Lashaka Sierra Hamlette, Melissa L. Caras

Correspondence

mcaras@umd.edu

In brief

Macedo-Lima et al. reveal that orbitofrontal cortex (OFC) inactivation disrupts task-dependent plasticity of auditory cortical neurons and impairs behavioral sound detection. These data indicate that the OFC facilitates rapid adjustments in auditory cortical sensitivity, ensuring that organisms are able to detect behaviorally relevant sounds.

Highlights

- Gerbil orbitofrontal cortex (OFC) neurons are sensitive to auditory task engagement
- OFC inactivation impairs behavioral sound detection
- OFC inactivation impairs task-dependent plasticity in auditory cortical neurons
- Auditory cortical sensitivity correlates with behavioral performance

Macedo-Lima et al., 2024, Current Biology *34*, 3354–3366
August 5, 2024
https://doi.org/10.1016/j.cub.2024.06.036

CellPress

CellPress

Current Biology

Article

Orbitofrontal cortex modulates auditory cortical sensitivity and sound perception in Mongolian gerbils

Matheus Macedo-Lima,[1] Lashaka Sierra Hamlette,[1] and Melissa L. Caras[1,2,*]
[1]Department of Biology, University of Maryland, College Park, MD 20742, USA
[2]Lead contact
*Correspondence: mcaras@umd.edu
https://doi.org/10.1016/j.cub.2024.06.036

SUMMARY

Sensory perception is dynamic, quickly adapting to sudden shifts in environmental or behavioral context. Although decades of work have established that these dynamics are mediated by rapid fluctuations in sensory cortical activity, we have a limited understanding of the brain regions and pathways that orchestrate these changes. Neurons in the orbitofrontal cortex (OFC) encode contextual information, and recent data suggest that some of these signals are transmitted to sensory cortices. Whether and how these signals shape sensory encoding and perceptual sensitivity remain uncertain. Here, we asked whether the OFC mediates context-dependent changes in auditory cortical sensitivity and sound perception by monitoring and manipulating OFC activity in freely moving Mongolian gerbils of both sexes under two behavioral contexts: passive sound exposure and engagement in an amplitude modulation (AM) detection task. We found that the majority of OFC neurons, including the specific subset that innervates the auditory cortex, were strongly modulated by task engagement. Pharmacological inactivation of the OFC prevented rapid context-dependent changes in auditory cortical firing and significantly impaired behavioral AM detection. Our findings suggest that contextual information from the OFC mediates rapid plasticity in the auditory cortex and facilitates the perception of behaviorally relevant sounds.

INTRODUCTION

Sensory perception is highly flexible, constantly adjusting to context-dependent changes in arousal,[1–4] attention,[5,6] or expectations about upcoming events.[7–12] This rapid flexibility favors the detection of important or informative stimuli, supporting improved communication, predator avoidance, and reproductive success.

Context-dependent shifts in perception are thought to result from rapid changes in sensory cortical processing. For instance, when a stimulus suddenly acquires behavioral relevance (such as when it must be used to solve a task), sensory cortical neurons quickly adjust their tuning properties, response strengths, and/or functional connectivity to optimize its detection, discrimination, or identification.[6,13–31] These data indicate that sensory cortices must receive signals that tell them when and how to adjust their activity, but where and how such signals are initiated remain unclear.

Several lines of evidence suggest that the orbitofrontal cortex (OFC) is particularly well positioned to mediate contextual signaling. First, the OFC is unique in that it is the only frontal cortical region to integrate inputs from all sensory modalities,[32,33] providing it a distinct vantage point for discerning shifts in environmental or behavioral demands. Second, in addition to their well-established role in encoding value,[34] OFC neurons also encode social,[35] spatial,[36,37] and behavioral contexts.[38–41] While recent work indicates that some of these signals are transmitted to sensory cortices,[38–41] their downstream impact on sensory encoding and perceptual sensitivity is only beginning to be understood.

Here, we asked whether the OFC shapes sound processing and perception by relaying contextual information to the auditory cortex in freely moving animals. We first recorded extracellular activity from OFC neurons under two different behavioral contexts: passive sound exposure and engagement in a sound detection task. We found that the majority of OFC neurons, including the specific subset that innervate the auditory cortex, exhibited context-dependent changes in firing rates. We then pharmacologically suppressed OFC activity during task engagement and assessed the effect on auditory perception and auditory cortical sound processing. OFC inactivation both impaired behavioral sound detection and prevented task-dependent changes of auditory cortical firing. Our findings suggest that the OFC supports context-dependent modulations of stimulus representations within the auditory cortex, contributing to the enhanced perception of behaviorally relevant sounds.

RESULTS

OFC neurons are sensitive to behavioral context

Auditory cortical neurons are more sensitive to amplitude-modulated (AM) stimuli when animals perform an AM detection task,

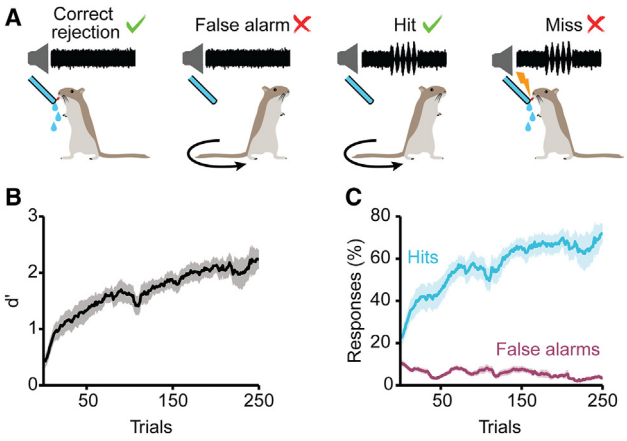

Figure 1. Behavioral task

(A) Task structure. Water-deprived animals were trained to drink from a waterspout, while unmodulated noise continuously played from a speaker, and to withdraw from the spout upon presentation of amplitude-modulated (AM) noise. Failing to withdraw during AM noise was punished with a mild shock.

(B and C) Mean ± standard error d' values (B) or hit rates and false alarm rates (C) for all animals included in this study ($n = 25$). Data were concatenated from training sessions over 12 days and analyzed using a 20-trial sliding window. Animals were only used for experiments after they reached expert performance levels ($d' \geq 2$).

compared with when the same sounds are presented in a passive, non-task context.[13] This finding, which is consistent with decades of work,[17,18,20,22,23,27,28,42–46] suggests that task engagement recruits non-sensory networks that modulate auditory cortical response properties. If OFC participates in this process, then we should also observe a neural signature of task engagement in OFC neurons.

To test this prediction, we trained Mongolian gerbils on the same AM detection task described above. In this task, animals must drink from a waterspout in the presence of unmodulated noise and withdraw from the spout when the sound transitions to an AM noise to avoid an aversive shock (Figure 1A). Animals learned the task quickly, reaching expert performance levels ($d' \geq 2$; STAR Methods) within 41–953 trials (median = 225 trials) across 3–18 sessions (median 5 days) (Figures 1B and 1C; $n = 25$ animals across all experiments; 13 females). We then implanted 5 of these animals (2 female) with 64-channel silicon probe arrays in the left OFC and recorded from 313 single units and 234 multi-units during task engagement and during passive sound exposure sessions just before ("passive-pre") and just after ("passive-post") the task (Figures 2A–2C). During passive exposure sessions, the spout was removed from the test arena and the shocker was turned off, but everything else, including the sound stimuli and position of the recording electrodes, remained identical to the task.

We first examined the effect of behavioral context on the tonic firing rates of OFC units during periods of unmodulated noise presentation, with the idea that changes in ongoing OFC activity could modulate the excitability (and subsequent sound-evoked responses) of auditory cortical neurons. For each unit, we used a Wilcoxon signed-rank test to ask whether firing rates during unmodulated noise differed between the passive-pre and task contexts (STAR Methods).

We found that most OFC units (411/547; 75%) were significantly modulated by context. Overall, 40% (217/547) were "task-suppressed," exhibiting reduced firing rates during the task, compared with the initial passive-pre session (Figure 2D). A roughly equal number (194/547 units, 35%) were "task-enhanced." The remaining units (136/547; 25%) were unaffected by context and were deemed "task-unchanged." A smooth continuum of context-dependent modulation was clearly observed (Figure 2E), similar to previous reports in the auditory cortex.[47] Moreover, the absolute magnitude of the context-dependent modulation was similar between task-suppressed and task-enhanced units ($p = 0.699$) and was (by definition) significantly lower in task-unchanged units ($p < 0.001$; Figure 2F).

The effect of task engagement on auditory cortical neurons can persist for several minutes or hours following task termination.[13,23–25,30,48] If the OFC mediates the changes observed in auditory cortex, OFC neurons should exhibit similar temporal dynamics. Therefore, we asked whether changes in tonic OFC activity persist into the passive sound exposure session immediately following the task. As shown in Figure 2G, the firing rates of task-enhanced units returned to passive-pre levels after the task was over ($p = 0.185$; see Table 1 for full statistical results). In contrast, task-suppressed units exhibited longer-lasting changes, such that firing rates during the passive-post session remained significantly lower than during the passive-pre session ($p < 0.001$). Task-unchanged units exhibited no changes in firing across the three sessions (all $p > 0.069$).

The data presented above suggest that context-dependent changes in tonic OFC firing could theoretically contribute to corresponding changes in sound-evoked activity in the auditory cortex. An additional route by which the OFC may exert an effect on auditory cortical sound sensitivity is via context-dependent changes in phasic firing during the presentation of the target AM noise stimulus. To explore this possibility, we examined OFC activity time-locked to AM sound onset by calculating the area under the receiver operating characteristic curve (auROC) from peristimulus time histograms[49] (Figures S1A–S1F). This approach is useful for comparing response dynamics across many units that differ widely in firing rate. auROC values range from 0 to 1, with values >0.5 indicative of increased firing and values <0.5 indicative of decreased firing. Neurons without spikes during the non-AM period ($n = 14$) were excluded from these analyses.

During passive exposure sessions, OFC firing was unremarkable, with auROC values consistently hovering around 0.5 and no obvious change evoked by AM noise. During task engagement, on the other hand, OFC units exhibited a heterogeneous array of responses, including both increases and decreases in auROC values following AM onset (Figure S1G). While some of these units may have been sensitive to the AM stimulus, the majority appeared to be particularly sensitive to trial outcome, with changes in firing sometimes lasting 2–4 s after AM onset. Similar findings were observed when we used fiber photometry to specifically monitor calcium signals in the OFC neurons that innervate the auditory cortex (Figures S1H–S1L).

To further explore these dynamics, we aligned OFC electrophysiological activity to the moment a behavioral response was initiated (spout withdrawal) and used the same auROC approach described above to calculate the magnitude of firing

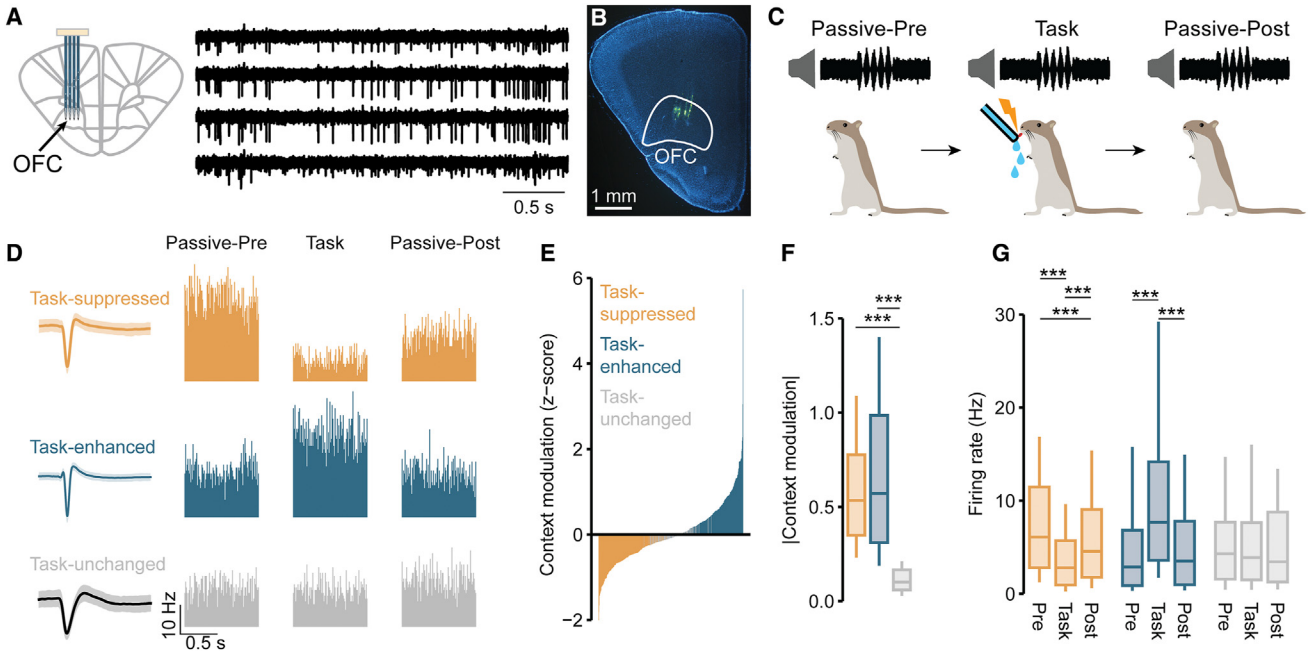

Figure 2. OFC neurons are sensitive to behavioral context

(A) Extracellular recordings were made from 64-channel electrode arrays chronically inserted into the left OFC. Sample recordings illustrate filtered voltage traces from four adjacent channels capturing activity from the same unit.

(B) Histological images were used to confirm electrode placement by visualizing fluorescently labeled tracks (green) in the OFC.

(C) OFC activity was recorded during task engagement and during passive sound exposure sessions just before (passive-pre) and just after (passive-post) the task. The same units were recorded across all three sessions.

(D) Peristimulus time histograms of three representative OFC units illustrate the effect of task engagement on non-AM firing rates. The task-suppressed unit (orange) exhibited a significant decrease in firing during the task, while the task-enhanced unit (teal) exhibited a significant decrease. The task-unchanged unit (gray) exhibited no change across sessions. Mean ± standard deviation waveforms for each unit are shown on the left.

(E) The magnitude of context modulation for each unit was calculated as the difference between the non-AM firing rate during the task and the non-AM firing rate during the passive-pre session *Z* scored over trials. Modulation values are presented for all units sorted in increasing order.

(F) Absolute modulation magnitudes were similar between task-enhanced and -suppressed units and significantly higher than in task-unchanged units. Boxplot center lines represent medians, boxes represent the 25%–75% interquartile range, and whiskers represent the 10%–90% interquartile range.

(G) Task-suppressed units exhibited reductions in non-AM firing that persisted into the passive-post period. The activity of task-enhanced units, on the other hand, returned to passive-pre levels after the task ended. The activity of task-unchanged units remained stable across sessions. Boxplots are as described for (F).

***$p < 0.001$.

See also Figure S1 and Table 1.

rate changes following the spout withdrawal. Because some units exhibited post-spout withdrawal increases in firing, while others exhibited decreases, we quantified the "phasic modulation" for each unit by subtracting 0.5 from each auROC value and taking the absolute value of the result. Phasic modulation values therefore ranged from 0 to 0.5, with 0 indicating no modulation and 0.5 indicating maximum modulation, regardless of the direction of change. We classified units as significantly modulated during this period if the mean phasic modulation exceeded the upper bound of the 95% confidence interval of the distribution. We found significant post-spout withdrawal modulations in the majority (278/533; 52%) of OFC units (Figures S2A and S2B). More units were modulated during hit (10% decrease, 38% increase) than during false alarm (5% decrease, 25% increase) or miss trials (7% decrease, 22% increase).

Across the population, average modulation values were larger on hit trials than on false alarms or miss trials (all $p < 0.001$), but they were similar between false alarms and misses ($p = 0.754$; Figure S2C). A similar pattern was observed if we performed the same analyses separately for units in each tonic modulation subcategory (task-enhanced, -suppressed, or -unchanged; Figures S3A and S3B). These data indicate that OFC neurons differentially encode trial outcome or behavioral choice. Although the timing of these signals suggests that they are unlikely to contribute to context-dependent signal enhancements on the current trial, they are well positioned to provide the auditory cortex with choice-dependent feedback that updates upcoming sensory representations on a trial-by-trial basis during learning, as previously proposed.[38–41,50]

In addition to post-spout withdrawal modulations, many OFC units also exhibited firing rate changes that *preceded* spout withdrawal (Figure 3A). On miss trials, animals failed to withdraw from the spout until they were shocked; thus, the moments leading up to spout withdrawal were always contaminated by a shock artifact. For this reason, we focused exclusively on hit and false alarm trials for this analysis. We found that many OFC units (180/533; 34%) exhibited significant modulations prior to spout

Table 1. Statistical results

Figure	Test	Factor(s)	Statistic	*p* value
Figure 2F	GLM/ANOVA	unit type	$\chi^2_2 = 431.990$	<0.001[a]
	Bonferroni: unit type	suppressed, enhanced	$t_{541} = -1.194$	0.699
		suppressed, unchanged	$t_{541} = 18.319$	<0.001[a]
		enhanced, unchanged	$t_{541} = 18.754$	<0.001[a]
Figure 2G	GLM/ANOVA: task-suppressed	context	$\chi^2_2 = 352.410$	<0.001[a]
	Bonferroni: context	pre, task	$t_{644} = -7.666$	<0.001[a]
		pre, post	$t_{644} = 6.051$	<0.001[a]
		task, post	$t_{644} = -6.244$	<0.001[a]
	GLM/ANOVA: task-enhanced	context	$\chi^2_2 = 368.830$	<0.001[a]
	Bonferroni: context	pre, task	$t_{575} = -17.511$	<0.001[a]
		pre, post	$t_{575} = -1.926$	0.164
		task, post	$t_{575} = 15.585$	<0.001[a]
	GLM/ANOVA: task-unchanged	context	$\chi^2_2 = 5.351$	0.069
Figure 3C	GLM/ANOVA	trial type	$\chi^2_1 = 49.281$	<0.001[a]
Figure 4C	GLM/ANOVA	treatment	$\chi^2_1 = 41.851$	<0.001[a]
Figure 4D	GLM/ANOVA	treatment	$\chi^2_1 = 1.895$	0.169
Figure 4E	GLM/ANOVA	treatment	$\chi^2_1 = 2.599$	0.107
Figure 4F	GLM/ANOVA	treatment	$\chi^2_1 = 9.578$	0.002[a]
Figure 4G	GLM/ANOVA	treatment	$\chi^2_1 = 84.366$	<0.001[a]
Figure 4H	GLM/ANOVA	treatment	$\chi^2_1 = 4.247$	0.039[a]
Figure 5C	GLM/ANOVA	treatment	$\chi^2_1 = 238.960$	<0.001[a]
Figure 5E	GLM/ANOVA: saline	context	$\chi^2_1 = 7.293$	0.007[a]
	GLM/ANOVA: muscimol	context	$\chi^2_1 = 1.952$	0.162
Figure 5F	GLM/ANOVA: saline	context	$\chi^2_1 = 8.280$	0.004[a]
	GLM/ANOVA: muscimol	context	$\chi^2_1 = 2.405$	0.121
Figure 5G	GLM/ANOVA: saline	context	$\chi^2_1 = 0.313$	0.576
	GLM/ANOVA: muscimol	context	$\chi^2_1 = 1.706$	0.192
Figure 5H	GLM/ANOVA: saline	context	$\chi^2_1 < 0.001$	0.978
	GLM/ANOVA: muscimol	context	$\chi^2_1 = 0.239$	0.625
Figure 6B	GLM/ANOVA	behavioral d'	$\chi^2_1 = 7.957$	0.005[a]
Figure 6C	GLM/ANOVA	behavioral performance	$\chi^2_1 = 11.526$	<0.001[a]

GLM, generalized linear model; ANOVA, analysis of variance.
[a]*p* values indicate statistical significance.

withdrawal and that more units were modulated on hit trials (6% decrease, 19% increase) than on false alarm trials (3% decrease, 16% increase; Figure 3B). Additionally, average modulation values were larger on hit trials (when the AM noise was present) than on false alarm trials (when the AM noise was not; Figure 3C; $p < 0.001$). Similar findings were observed if we performed the same analyses separately for units in each tonic modulation subcategory (Figure S3C). These findings raise the possibility that firing rate modulations leading to spout withdrawal may (at least in part) be acoustically driven, which suggests that OFC neurons generate phasic signals within time frames relevant for online AM detection (i.e., before a behavioral action is performed). These signals may serve to further (and specifically) boost the AM-evoked signal in the auditory cortex during task performance, thereby enhancing target sound detection.

Collectively, these data reveal that in addition to encoding trial outcome, a subset of OFC neurons exhibits context-dependent modulations in tonic firing that evolve over a similar time course as the modulations observed in the auditory cortex and also exhibits phasic firing rate changes that precede spout withdrawal. These tonic and phasic modulations could work in concert to enhance the detection of behaviorally relevant sounds in the auditory cortex.

OFC inactivation impairs AM detection behavior

Task-dependent modulation of the auditory cortex is believed to enhance the detection or discrimination of behaviorally relevant stimuli.[13,17,18,20,22,23,27,28,42–47] If the OFC mediates task-dependent modulations in the auditory cortex, then suppressing OFC activity should impair sound detection. To test this prediction, we implanted cannulas in bilateral OFC of nine gerbils (six females) previously trained to detect AM stimuli. In one male and one female, right hemisphere infusion cannulas clogged, but data from these animals were still included to evaluate the effect of unilateral left OFC inactivation. On alternating days, we infused either saline or muscimol (a $GABA_a$ agonist

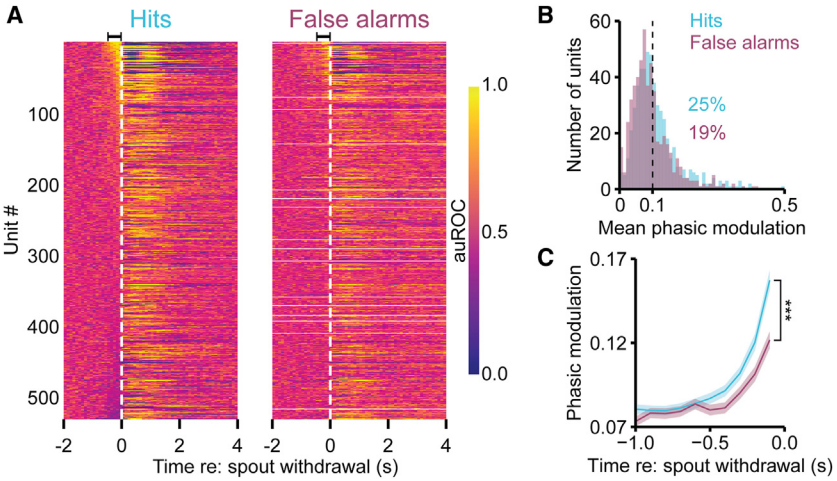

Figure 3. OFC neurons exhibit firing rate modulations that precede spout withdrawal

(A) Heatmaps illustrate normalized neuronal firing (auROC) aligned to spout withdrawal (time = 0 s; vertical dashed white lines). auROC values range from 0 to 1, with values >0.5 indicative of increased firing and values <0.5 indicative of decreased firing. Units without spikes during the non-AM period were excluded from these analyses. Data are from 309 single units and 224 multi-units. OFC units (rows) are ordered by the mean auROC between −0.5 and 0 s (brackets on top of heatmaps) during hit trials, and the same order is used for false alarm trials. On miss trials, animals failed to withdraw from the spout until they were shocked; thus, the moments leading up to spout withdrawal were always contaminated by a shock artifact. For this reason, we focused exclusively on hit and false alarm trials for this analysis. Solid white rows are from sessions during which auROC could not be calculated because of an absence of spiking.

(B) Histograms illustrate the distribution of mean phasic modulation within the 0.5-s window preceding the spout withdrawal during hits and false alarms. Phasic modulation values were calculated as |auROC − 0.5|. Values range from 0 (no modulation) to 0.5 (maximum modulation). Units were classified as significantly modulated if mean phasic modulation was above the 95% confidence interval of the distribution (dashed line). Percentages indicate the proportion of units with significant phasic modulation.

(C) Mean phasic modulation values in the 0.5 s preceding spout withdrawal (illustrated as mean ± standard error across units) were larger on hit trials than on false alarm trials. ***$p < 0.001$.

See also Figures S2 and S3 and Tables 1 and S1.

that reversibly silences neural activity) into the OFC shortly before animals performed the AM detection task (Figures 4A and 4B).

OFC inactivation significantly impaired AM detection. As shown in Figure 4C, behavioral d' values were lower (poorer) in all animals tested after muscimol was infused into the OFC, compared with when saline was infused ($p < 0.001$; see Table 1 for full statistical results). Impaired performance could not be explained by reduced motivation to engage in the task, as the amount of water consumed (Figure 4D) and the number of AM trials completed (Figure 4E) were unaffected by muscimol infusion (both $p > 0.1$). However, OFC inactivation did reduce the rate of trial completion ($p = 0.002$; Figure 4F). This observation might be explained by the fact that the poor performance caused by muscimol infusion resulted in animals receiving more frequent punishment, thereby generating more frequent (and longer) spout withdrawals. Indeed, miss rates strongly predicted rates of trial completion ($p < 0.001$; Figure S4A).

OFC inactivation may have impaired behavioral performance by disrupting an animal's ability to detect the AM sound cue (thereby reducing the hit rate) and/or by increasing indiscriminate responding to the unmodulated noise (thereby increasing the false alarm rate). This latter scenario is important to consider, as OFC lesions have been associated with changes in impulsive behavior.[51,52] To address this issue, we asked how muscimol infusion separately impacted hit rates and false alarm rates. We found that muscimol treatment drastically reduced hit rates in all animals tested ($p < 0.001$; Figure 4G). In contrast, muscimol treatment only modestly increased false alarm rates ($p = 0.039$; Figure 4H). This small uptick in false alarm rates might be explained by the fact that animals that receive more frequent punishment are more hesitant to stay on the spout. Indeed, miss rates strongly predicted false alarm rates ($p = 0.001$; Figure S4B). Collectively, these observations suggest that after OFC inactivation, animals struggle to detect AM noise.

OFC inactivation prevents contextual modulation of auditory cortical neurons

Task-dependent modulations of auditory cortical activity are not fixed in magnitude, and their strength correlates with behavioral AM detection abilities. Strong modulations are associated with excellent AM detection skills, whereas small modulations are associated with poor performance.[13] This observation, together with the findings presented above, raises the possibility that OFC inactivation impairs behavioral AM detection by disrupting task-dependent modulations of auditory cortical activity.

To test this hypothesis, we implanted three gerbils (one male) with cannulas in bilateral OFC and a 64-channel silicon probe in left auditory cortex. We initially recorded 22 single units and 45 multi-units in layer 2/3 of the auditory cortex during passive sound exposure. We then infused saline or muscimol into the OFC and recorded from the same auditory cortical units as the animals performed the AM detection task (Figure 5A; saline, $n = 28$; muscimol, $n = 39$ units). Electrode tracks were visualized offline and used to reconstruct recording site locations (Figure 5B).

We first confirmed that OFC inactivation impaired behavioral performance in these animals. As expected from our previous findings, muscimol infusion reduced behavioral d' values ($p < 0.001$; Figure 5C) and hit rates ($p = 0.004$; Figure S5A) in all subjects without significantly affecting false alarm rates or water consumption (all $p > 0.099$; Figures S5B and S5C). We then asked how OFC inactivation affected auditory cortical activity. Figure 5D illustrates AM-evoked responses from two representative auditory cortical units from the same animal recorded on

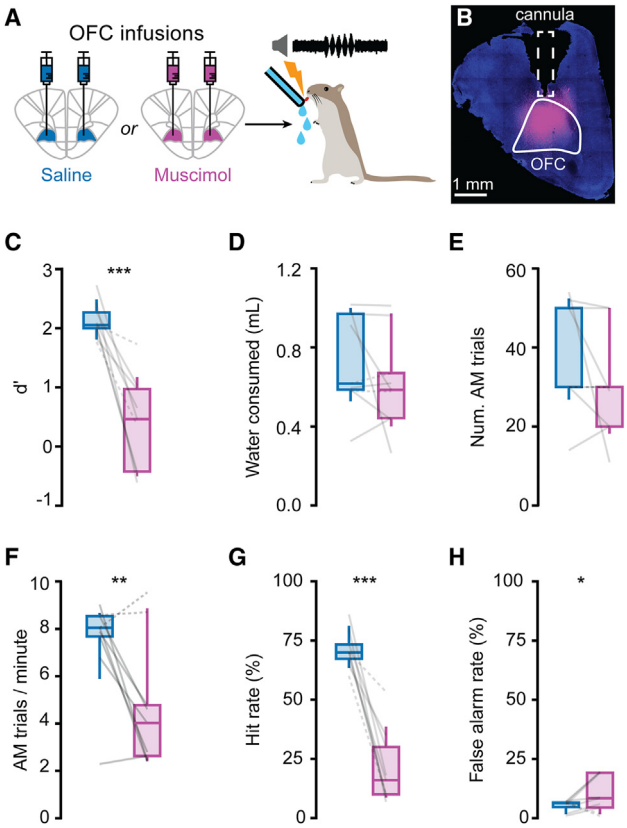

Figure 4. OFC inactivation impairs AM detection behavior

(A) On alternating days, muscimol or saline was infused into bilateral OFC ~40 min before animals performed the AM detection task.

(B) At the conclusion of the experiment, a fluororuby infusion just prior to transcardial perfusion provided an estimation of drug spread.

(C–F) Muscimol infusions reduced behavioral d' values (C), without systematically affecting water consumption (D) or the number of completed AM trials (E). However, muscimol infusion did reduce the rate of AM trial completion (F). Boxplot center lines represent medians, boxes represent the 25%–75% interquartile range, and whiskers represent the 10%–90% interquartile range.

(G and H) Muscimol infusions significantly reduced hit rates (G) and only slightly increased false alarm rates (H). Dashed lines indicate data from animals that received unilateral left infusions due to partially clogged cannulas. Boxplots are as described for (C)–(F). $^{*}p < 0.05$, $^{**}p < 0.01$, $^{***}p < 0.001$.

See also Figure S4 and Tables 1 and S1.

different days. The responses in the top row were recorded from one unit before and after saline infusion into the OFC. This unit showed a stronger AM-evoked firing rate during the task than during passive sound exposure, consistent with our previously published work.[13] In contrast, the responses in the bottom row, which were recorded from a different unit before and after muscimol infusion into the OFC, showed a moderately reduced firing rate following OFC inactivation.

To determine whether these differences in response gain translated into differences in AM sensitivity, we transformed the firing rates of individual units into a neural discriminability metric (neural d'), using our previously established approach.[13,53] We report absolute neural d' values here because negative d' values can also support enhanced AM detection via decreases in firing relative to baseline. When saline was infused into OFC, absolute neural d' values were significantly higher during task engagement than during passive sound exposure ($p = 0.007$; Figure 5E), as expected from our prior work.[13] In contrast, when muscimol was infused into the OFC, absolute neural d' values during task engagement and passive sound exposure were similar ($p = 0.162$). These data demonstrate that suppressing the OFC prevents task-dependent modulations of the auditory cortex.

The d' value for each unit depends on its average firing rate and its firing rate variability during non-AM and AM noise (supplemental information). To determine which of these factors are impacted by OFC inactivation, we first examined the firing rates of individual units and compared these values between passive and task sessions. We found that task engagement did not systematically affect auditory cortical firing rates evoked by either non-AM or AM noise, regardless of drug treatment (all $p > 0.1$; Figures S6A and S6B). This observation raised the possibility that the differences we observed in neural d' values are due to joint changes in non-AM and AM noise responses that manifest on a unit-by-unit basis (STAR Methods).[13] To test this idea, we calculated the difference between AM and non-AM firing rates for each auditory cortical unit (here termed the ΔFR), and we then compared ΔFR values between passive and task sessions. We found that ΔFR significantly increased during task engagement when saline was infused into the OFC ($p = 0.004$). In contrast, ΔFR values remained similar between sessions when muscimol was infused ($p = 0.121$; Figure 5F).

We then calculated the coefficient of variation (CV) for each unit as an indicator of firing rate variability and compared CV values between passive and task sessions. Task engagement did not significantly affect non-AM- or AM-evoked CV values, regardless of drug treatment (all $p > 0.4$; Figures S6C and S6D), nor did it affect the sum of non-AM and AM CV values (all $p > 0.192$; Figure 5G). Together, these findings suggest that OFC inactivation prevents a task-dependent increase in the separation of AM and non-AM firing rate distributions and not a task-dependent reduction in firing rate variability.

In addition to modulating average firing rates, task engagement can also impact sound encoding and perception by enhancing stimulus phase-locking.[27,43] Therefore, we calculated the phase-projected vector strength evoked by AM noise for individual auditory cortical units and compared these values between passive and task sessions.[27,43,54] We found that task engagement had no effect on vector strength regardless of drug treatment (all $p > 0.625$; Figure 5H). This finding is consistent with the observation that task-dependent effects on phase-locking are more significant when AM depths are small.[27]

Collectively, these results indicate that OFC inactivation prevents context-dependent enhancements of behaviorally relevant sound representations in the auditory cortex by modifying neuronal firing rates, without affecting neuronal phase-locking.

Auditory cortical AM sensitivity correlates with behavioral performance

In two subjects (one female) chronically implanted with OFC cannulas and auditory cortex electrodes, we infused saline or muscimol into the OFC multiple times over several days in an attempt to enlarge our sample of auditory cortical units. However, we noticed that the effectiveness of repeated muscimol infusions

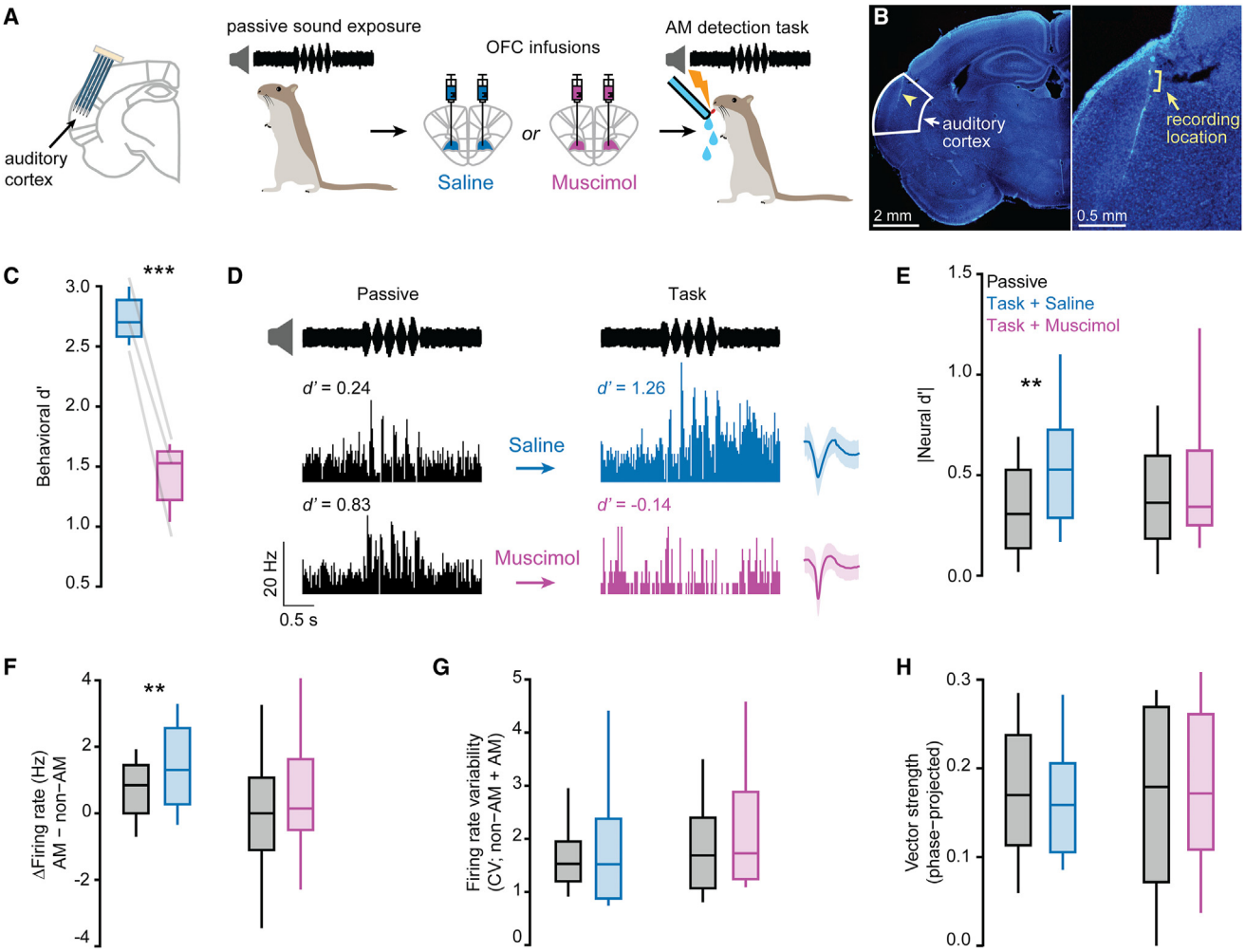

Figure 5. OFC inactivation prevents contextual modulation of auditory cortical neurons

(A) Auditory cortical multi-units and single units were chronically recorded while animals were passively exposed to sounds. Animals then received muscimol or saline infusions in bilateral OFC. Following the infusions, recordings were again made from the same auditory cortical units while animals performed the AM detection task.

(B) Electrode placement was confirmed to be in auditory cortex by visualizing fluorescently labeled tracks (green) post-mortem. Recording sites were estimated to be in layers 2/3 (brackets in inset).

(C) OFC inactivation impaired behavioral AM detection, replicating the results presented in Figure 4. Boxplot center lines represent medians, boxes represent the 25%–75% interquartile range, and whiskers represent the 10%–90% interquartile range.

(D) AM-evoked responses are shown from two representative auditory cortical units recorded from the same animal on different days. Top: an auditory cortical unit recorded before and after saline infusion into the OFC exhibits stronger AM-evoked firing during the task than during passive sound exposure, consistent with our previously published work.[13] Bottom: an auditory cortical unit recorded before and after muscimol infusion into the OFC exhibits a modestly reduced firing rate during the task, compared with passive sound exposure.

(E and F) OFC inactivation prevents a task-dependent increase in auditory cortical neural d' values (E) and prevents a task-dependent increase in the separation of AM and non-AM firing rate distributions (F). This separation (termed Δfiring rate) was calculated for each unit as the difference between AM-evoked and non-AM-evoked firing rates. Boxplots are as described for (C).

(G and H) Neither task engagement nor OFC inactivation affected firing rate variability (G) or phase-locking (H). Boxplots are as described for (C). $^{**}p < 0.01$, $^{***}p < 0.001$.

See also Figures S5 and S6 and Tables 1 and S1.

quickly waned and ultimately failed to significantly impact behavior (Figure 6A), suggestive of a compensatory mechanism after whole-session OFC inactivation.

We took advantage of this variability to ask whether muscimol's effectiveness, inferred from downstream auditory cortical AM sensitivity, predicted behavioral AM detection. We recorded from 60 single units and 96 multi-units from the auditory cortex over 10 days. Indeed, behavioral d' values significantly correlated with neural d' values during the task ($p = 0.002$; Figure 6B). To highlight this relationship, we compared neural d' values from the two worst performance days from each animal with the two best days (regardless of drug treatment). We found that neural d' values were significantly higher when behavioral performance was good than when performance was poor ($p < 0.001$; Figure 6C).

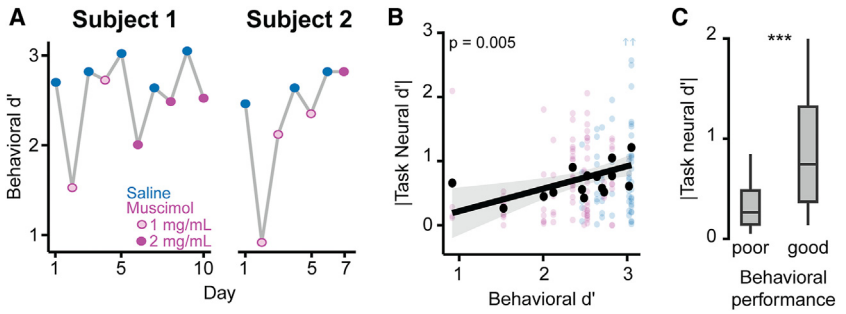

Figure 6. Auditory cortical AM sensitivity correlates with behavioral performance

(A) Repeated muscimol injections into bilateral OFC exert progressively weaker effects on behavior in two subjects. Doubling the muscimol concentration (dark magenta) modestly restored the behavioral effect in one subject (left).

(B) Absolute neural d' values for individual auditory cortical units (small translucent points) are plotted as a function of the behavioral d' value obtained during the recording session. Black points illustrate median absolute neural d' for each behavioral d' value. Blue arrows indicate two points that exceeded the depicted range of neural d' values. Neural and behavioral d' values are significantly correlated.

(C) Absolute neural d' values obtained during the task were significantly higher on days when behavioral performance was good (two best days from each animal) versus days when behavioral performance was poor (two worst days from each animal). n = 30 units on poor performance days and n = 49 units on good performance days. Boxplot center lines represent medians, boxes represent the 25%–75% interquartile range, and whiskers represent the 10%–90% interquartile range. ***$p < 0.001$.

See also Table 1.

These findings suggest that OFC is a key part of a distributed network that provides contextual information to the auditory cortex, and when OFC activity is repeatedly suppressed, other brain regions may be recruited to compensate for the loss.

DISCUSSION

Context-dependent modulation is a widely reported feature of the auditory cortex and is hypothesized to adaptively modify the perceptual salience of stimuli in response to moment-to-moment changes in their behavioral relevance.[13,17,18,20,22,23,27,28,42–47] Although prior work has identified several brain regions capable of modifying auditory cortical responses and behavior,[40,47,55–57] our understanding of the neural networks that mediate rapid shifts in auditory perception remains limited. In this study, we reveal that a subset of OFC neurons is sensitive to behavioral context, exhibiting task-dependent dynamics that mirror those previously observed in the auditory cortex.[13,23–25,30,48] Our pharmacological experiments demonstrate that OFC inactivation prevents task-dependent enhancements of auditory cortical sensitivity and in turn impairs the ability of animals to detect AM noise. Notably, the behavioral effect of repeated whole-session OFC inactivation gradually waned, suggesting that compensatory brain regions may be recruited when OFC output is unavailable. Together, our results suggest that OFC provides contextual information to the auditory cortex to facilitate the perception of behaviorally relevant sounds.

Potential circuit mechanisms supporting auditory cortical plasticity

Our data suggest that the OFC plays a key role in transmitting contextual information to the auditory cortex to shape sound perception, but the route(s) by which such information is transmitted and the mechanisms by which it impacts auditory cortical processing remain uncertain. Several recent studies support the involvement of a monosynaptic pathway. For example, OFC axon terminals in the auditory cortex are sensitive to listening condition.[41] These terminals synapse onto both excitatory and inhibitory neurons,[58] and their stimulation reshapes auditory cortical frequency tuning in anesthetized mice.[58] These observations suggest that the task-dependent shifts in tonic OFC firing we report here could increase stimulus salience by disrupting the balance of excitation and inhibition in the auditory cortex. Given that the temporal dynamics of task-dependent changes in the auditory cortex match those of our task-suppressed OFC population, one intriguing possibility is that task-suppressed OFC neurons increase auditory cortical excitability and enhance signal detection by engaging a local disinhibitory microcircuit within the auditory cortex.[47,59,60]

Task-dependent shifts in tonic OFC firing may also (or instead) support auditory cortical plasticity via multi-synaptic pathways that recruit neuromodulatory centers. For instance, cholinergic input from the nucleus basalis alters auditory cortical receptive fields and sound perception, and cholinergic axons increase their tonic activity during sound-guided behavior.[47,59,61–64] Similarly, task engagement modulates tonic locus coeruleus (LC) activity and noradrenergic tone,[65] and both noradrenergic input from the LC and dopaminergic input from the ventral tegmental area (VTA) influence thalamocortical gain and receptive field organization in the auditory cortex.[55,66–71] The OFC projects to nucleus basalis,[32,72] LC,[73] and VTA[74] and regulates VTA firing.[75] Thus, OFC neurons may indirectly shape signal detection by relaying contextual information to cholinergic or monoaminergic neurons that innervate the auditory cortex. Targeted manipulations of OFC axons in neuromodulatory nuclei are needed to resolve these possibilities.

In addition to context-dependent modulations of tonic OFC activity, we found that during task performance, some OFC neurons exhibit phasic firing rate changes that preceded spout withdrawal by as much as 500 ms. This activity may represent expectations about upcoming task events (like an impending shock). However, the fact that these changes were larger on hit trials (when an AM noise was present) than on false alarm trials (when an AM noise was absent) suggests that they may (at least in part) be acoustically driven. This finding, which is consistent with prior reports,[41] raises the interesting possibility that recurrent excitation between the auditory cortex and OFC may serve to amplify the AM-evoked signal in the auditory cortex during task performance, thereby enhancing stimulus detection.[76,77] A more detailed anatomical study of the reciprocal connectivity

between OFC and auditory cortical neurons and experiments that silence those connections in a temporally specific manner are required to test this hypothesis.

As expected from prior work,[41] we found that OFC neurons, including those that innervate the auditory cortex, also generate signals that represent trial outcomes or behavioral choices. The timing of these signals (i.e., after a behavioral response) suggests that rather than participating in context-dependent enhancements of online sound detection, they provide the auditory cortex with feedback that updates sensory representations on a trial-by-trial basis. This feedback may support other forms of auditory plasticity such as learning, an idea in line with previous reports[38–41,50] and current theories[78] about the OFC's role in credit assignment[79–81] and prediction error coding.[82]

Comparison with prior findings and established roles of the OFC in regulating behavior

A primary finding of this study is that OFC inactivation significantly impairs behavioral AM detection. This result is seemingly at odds with a recent study by Banerjee et al. showing no impact of OFC silencing on expert performance in a tactile go/no-go task.[38] However, it is critical to consider a key difference between our behavioral paradigms. In Banerjee et al.'s study, tactile cues were always preceded by a tone; thus, the mice knew exactly when the stimulus of interest would be presented. Our paradigm, on the other hand, asked animals to report when an ongoing noise unpredictably changed from an unmodulated signal to an AM signal. Therefore, OFC inactivation may have compromised expert behavioral performance on our task not just by preventing task-dependent enhancements in auditory cortical sensitivity but also by impairing the ability of animals to maintain a high level of vigilance. This idea is consistent with prior reports highlighting the OFC's role in attention[83–85] (but see McAlonan and Brown[86]).

Our findings are also in agreement with a recent study examining the role of the OFC in aversive fear conditioning.[81] In this study, rats were trained to discriminate between two highly salient sensory stimuli: a conditioned fear stimulus (CS+) that was paired with a shock and a conditioned safety stimulus (CS−) that was not. Animals were then tested on their ability to recall the learned associations and discriminate the stimuli. The authors found that an infusion of muscimol into the OFC significantly impaired stimulus discrimination during the recall test, similar to the deficit we observed in our aversive go/no-go task. However, if muscimol was infused prior to the initial conditioning, no effect was observed—associative learning progressed normally, similar to what Banerjee et al.[38] and others[80,87–90] have reported. The authors interpreted these data to mean that the OFC is necessary for tracking and responding to changing expectations of danger, as during the recall tests, the CS+ and CS− were presented sequentially in an unpredictable manner. This interpretation, which is consistent with the OFC's well-established role in regulating behavioral flexibility,[91] could also be applied to our data.

Caveats of the current study

We relied on muscimol infusions to inactivate the OFC, but we did not employ additional physiological verifications to evaluate the spread of the drug. Therefore, some of our effects may be partly explained by inactivation of nearby brain regions. The prelimbic and infralimbic cortices would be of particular interest, given their known involvement in auditory attention and deviance detection.[92,93] Given that we used fluororuby to estimate the spatial extent of the infusions and that the dye appeared to be restricted to the OFC, we find it unlikely that off-target spread made a substantial contribution to our findings, but we cannot rule it out entirely.

An unexpected finding that emerged from our experiments was that the effect of repeated OFC inactivation waned across days. One obvious possibility is that the chemical solution lost its potency (i.e., the muscimol "went bad") after 1 or 2 days. We do not believe this to be the likely explanation, as aliquots were frozen and used within 1 month of dilution, as recommended by the manufacturer. Another possibility is that rather than generating a negative effect on sound processing and perception, the first muscimol infusion generated a novel "internal experience" that caused animals to initially perform poorly, and repeated infusions allowed animals to habituate to this experience and ultimately perform well. We also find this scenario unlikely, as auditory cortical AM sensitivity tracked behavioral AM sensitivity throughout the course of repeated OFC inactivation, and there is no reason to believe the effects of a novel internal experience would manifest as reduced sound sensitivity in the auditory cortex. Instead, we believe the most parsimonious explanation is that when OFC output is repeatedly unavailable, compensatory brain regions are recruited to restore auditory cortical and perceptual sensitivity.

Implications for perceptual learning

We previously found that task-dependent modulations of auditory cortical neurons grow stronger as animals learn to detect small, near-threshold AMs.[13] This observation suggests that the non-sensory inputs that rapidly modulate auditory cortical activity during task performance also mediate the gradual, longer-term plasticity processes that underlie perceptual learning. This idea is supported by human behavioral experiments demonstrating that in some cases, perceptual learning can be generated by interleaving brief bouts of practice (which are too short to drive learning on their own) with passive sound exposure.[94] These data suggest that (1) the non-sensory processes engaged by task performance remain active for some time after task performance ends and (2) if sounds are passively presented during these periods of residual non-sensory activity, learning can occur. This interpretation closely matches our neurophysiological findings: both auditory cortical[13] and a subset of OFC neurons exhibit task-dependent changes in activity that persists for several minutes after the task has ended. Taken together, these findings support a conceptual framework that task engagement puts sensory cortical neurons into a "sensitized" state permissive for learning, which lasts for many minutes beyond the end of the task.[13,23,95,96] The neural circuits involved in regulating this phenomenon are still unclear, but our data suggest that a subpopulation of OFC neurons may be involved. Future work should use viral approaches to identify the downstream targets of these neurons and to determine their causal contributions to task-induced sensitization of sensory circuits and practice-based improvements in auditory perception.

STAR★METHODS

Detailed methods are provided in the online version of this paper and include the following:

- KEY RESOURCES TABLE
- RESOURCE AVAILABILITY
  - Lead contact
  - Materials availability
  - Data and code availability
- EXPERIMENTAL MODEL AND SUBJECT DETAILS
  - Subjects
- METHOD DETAILS
  - Choice of behavioral task
  - Behavioral set up
  - Behavioral training and testing
  - Electrode implant procedures
  - Electrophysiology
  - Fiber photometry
  - Brain cannulation and infusions
  - Histology and imaging
- QUANTIFICATION AND STATISTICAL ANALYSIS

SUPPLEMENTAL INFORMATION

Supplemental information can be found online at https://doi.org/10.1016/j.cub.2024.06.036.

ACKNOWLEDGMENTS

We thank the current and former members of the Caras Lab for helpful feedback and discussions and assistance with animal care. Special thanks to Dr. Daniel Stolzberg for assistance with software for behavioral testing. We acknowledge the Imaging Core Facility in the Department of Cell Biology and Molecular Genetics at the University of Maryland, College Park for training and the use of the Zeiss LSM 980 Airyscan 2 confocal microscope. Purchase of the Zeiss LSM 980 Airyscan 2 was supported by award no. 1S10OD025223-01A1 from the National Institutes of Health (NIH). This work was supported by NIH R00DC016046 and R01DC020742 to M.L.C.

AUTHOR CONTRIBUTIONS

M.M.-L., L.S.H., and M.L.C. designed research. M.M.-L. and L.S.H. performed research. M.M.-L. analyzed data. M.M.-L. and M.L.C. wrote the paper.

DECLARATION OF INTERESTS

The authors declare no competing interests.

Received: January 5, 2024
Revised: April 25, 2024
Accepted: June 12, 2024
Published: July 11, 2024

REFERENCES

1. Asutay, E., and Västfjäll, D. (2012). Perception of loudness is influenced by emotion. PLOS One *7*, e38660. https://doi.org/10.1371/journal.pone.0038660.
2. Kim, D., Lokey, S., and Ling, S. (2017). Elevated arousal levels enhance contrast perception. J. Vision *17*, 14. https://doi.org/10.1167/17.2.14.
3. Mather, M., and Sutherland, M.R. (2011). Arousal-biased competition in perception and memory. Perspect. Psychol. Sci. *6*, 114–133. https://doi.org/10.1177/1745691611400234.
4. McGinley, M.J., David, S.V., and McCormick, D.A. (2015). Cortical membrane potential signature of optimal states for sensory signal detection. Neuron *87*, 179–192. https://doi.org/10.1016/j.neuron.2015.05.038.
5. Shinn-Cunningham, B.G. (2008). Object-based auditory and visual attention. Trends Cogn. Sci. *12*, 182–186. https://doi.org/10.1016/j.tics.2008.02.003.
6. Spitzer, H., Desimone, R., and Moran, J. (1988). Increased attention enhances both behavioral and neuronal performance. Science *240*, 338–340. https://doi.org/10.1126/science.3353728.
7. Ashton, R.H. (2014). "Nothing Good Ever Came from New Jersey": expectations and the sensory perception of wines. J. Wine Econ. *9*, 304–319. https://doi.org/10.1017/jwe.2014.28.
8. Carcea, A.I., Insanally, M.N., and Froemke, R.C. (2017). Dynamics of cortical activity during behavioral engagement and auditory perception. Nat. Commun. *8*, 1–12. https://doi.org/10.1038/ncomms14412.
9. De Lange, F.P., Heilbron, M., and Kok, P. (2018). How do expectations shape perception? Trends Cogn. Sci. *22*, 764–779. https://doi.org/10.1016/j.tics.2018.06.002.
10. Pinto, Y., Van Gaal, S., De Lange, F.P., Lamme, V.A.F., and Seth, A.K. (2015). Expectations accelerate entry of visual stimuli into awareness. J. Vision *15*, 13. https://doi.org/10.1167/15.8.13.
11. Stein, T., and Peelen, M.V. (2015). Content-specific expectations enhance stimulus detectability by increasing perceptual sensitivity. J. Exp. Psychol. Gen. *144*, 1089–1104. https://doi.org/10.1037/xge0000109.
12. Vangkilde, S., Coull, J.T., and Bundesen, C. (2012). Great expectations: temporal expectation modulates perceptual processing speed. J. Exp. Psychol. Hum. Percept. Perform. *38*, 1183–1191. https://doi.org/10.1037/a0026343.
13. Caras, M.L., and Sanes, D.H. (2017). Top-down modulation of sensory cortex gates perceptual learning. Proc. Natl. Acad. Sci. USA *114*, 9972–9977. https://doi.org/10.1073/pnas.1712305114.
14. Chapman, C.E., and Meftah, E.-M. (2005). Independent controls of attentional influences in primary and secondary somatosensory cortex. J. Neurophysiol. *94*, 4094–4107. https://doi.org/10.1152/jn.00303.2005.
15. Cohen, M.R., and Maunsell, J.H.R. (2009). Attention improves performance primarily by reducing interneuronal correlations. Nat. Neurosci. *12*, 1594–1600. https://doi.org/10.1038/nn.2439.
16. David, S.V., Fritz, J.B., and Shamma, S.A. (2012). Task reward structure shapes rapid receptive field plasticity in auditory cortex. Proc. Natl. Acad. Sci. USA *109*, 2144–2149. https://doi.org/10.1073/pnas.1117717109.
17. Davis, H. (1964). Enhancement of evoked cortical potentials in humans related to a task requiring a decision. Science *145*, 182–183. https://doi.org/10.1126/science.145.3628.182.
18. De Franceschi, G., and Barkat, T.R. (2021). Task-induced modulations of neuronal activity along the auditory pathway. Cell Rep. *37*, 110115. https://doi.org/10.1016/j.celrep.2021.110115.
19. Downer, J.D., Rapone, B., Verhein, J., O'Connor, K.N., and Sutter, M.L. (2017). Feature-selective attention adaptively shifts noise correlations in primary auditory cortex. J. Neurosci. *37*, 5378–5392. https://doi.org/10.1523/JNEUROSCI.3169-16.2017.
20. Downer, J.D., Niwa, M., and Sutter, M.L. (2015). Task engagement selectively modulates neural correlations in primary auditory cortex. J. Neurosci. *35*, 7565–7574. https://doi.org/10.1523/JNEUROSCI.4094-14.2015.
21. Fontanini, A., and Katz, D.B. (2006). State-dependent modulation of time-varying gustatory responses. J. Neurophysiol. *96*, 3183–3193. https://doi.org/10.1152/jn.00804.2006.
22. Francis, N.A., Winkowski, D.E., Sheikhattar, A., Armengol, K., Babadi, B., and Kanold, P.O. (2018). Small networks encode decision-making in primary auditory cortex. Neuron *97*, 885–897.e6. https://doi.org/10.1016/j.neuron.2018.01.019.
23. Fritz, J., Shamma, S., Elhilali, M., and Klein, D. (2003). Rapid task-related plasticity of spectrotemporal receptive fields in primary auditory cortex. Nat. Neurosci. *6*, 1216–1223. https://doi.org/10.1038/nn1141.

24. Fritz, J.B., Elhilali, M., David, S.V., and Shamma, S.A. (2007). Auditory attention - focusing the searchlight on sound. Curr. Opin. Neurobiol. *17*, 437–455. https://doi.org/10.1016/j.conb.2007.07.011.

25. Fritz, J.B., Elhilali, M., and Shamma, S.A. (2005). Differential dynamic plasticity of A1 receptive fields during multiple spectral tasks. J. Neurosci. *25*, 7623–7635. https://doi.org/10.1523/JNEUROSCI.1318-05.2005.

26. Hubel, D.H., Henson, C.O., Rupert, A., and Galambos, R. (1959). "Attention" units in the auditory cortex. Science *129*, 1279–1280. https://doi.org/10.1126/science.129.3358.1279.

27. Niwa, M., Johnson, J.S., O'Connor, K.N., and Sutter, M.L. (2012). Active engagement improves primary auditory cortical neurons' ability to discriminate temporal modulation. J. Neurosci. *32*, 9323–9334. https://doi.org/10.1523/JNEUROSCI.5832-11.2012.

28. Sheikhattar, A., Miran, S., Liu, J., Fritz, J.B., Shamma, S.A., Kanold, P.O., and Babadi, B. (2018). Extracting neuronal functional network dynamics via adaptive Granger causality analysis. Proc. Natl. Acad. Sci. USA *115*, E3869–E3878. https://doi.org/10.1073/pnas.1718154115.

29. Steinmetz, P.N., Roy, A., Fitzgerald, P.J., Hsiao, S.S., Johnson, K.O., and Niebur, E. (2000). Attention modulates synchronized neuronal firing in primate somatosensory cortex. Nature *404*, 187–190. https://doi.org/10.1038/35004588.

30. Yin, P., Fritz, J.B., and Shamma, S.A. (2014). Rapid spectrotemporal plasticity in primary auditory cortex during behavior. J. Neurosci. *34*, 4396–4408. https://doi.org/10.1523/JNEUROSCI.2799-13.2014.

31. Yoshida, T., and Katz, D.B. (2011). Control of prestimulus activity related to improved sensory coding within a discrimination task. J. Neurosci. *31*, 4101–4112. https://doi.org/10.1523/JNEUROSCI.4380-10.2011.

32. Gao, L., Liu, S., Gou, L., Hu, Y., Liu, Y., Deng, L., Ma, D., Wang, H., Yang, Q., Chen, Z., et al. (2022). Single-neuron projectome of mouse prefrontal cortex. Nat. Neurosci. *25*, 515–529. https://doi.org/10.1038/s41593-022-01041-5.

33. Uylings, H.B.M., and Van Eden, C.G. (1990). Chapter 3 Qualitative and quantitative comparison of the prefrontal cortex in rat and in primates, including humans. Prog. Brain Res. *85*, 31–62. https://doi.org/10.1016/S0079-6123(08)62675-8.

34. Enel, P., Perkins, A.Q., and Rich, E.L. (2021). Heterogeneous value coding in orbitofrontal populations. Behav. Neurosci. *135*, 245–254. https://doi.org/10.1037/bne0000457.

35. Azzi, J.C.B., Sirigu, A., and Duhamel, J.-R. (2012). Modulation of value representation by social context in the primate orbitofrontal cortex. Proc. Natl. Acad. Sci. USA *109*, 2126–2131. https://doi.org/10.1073/pnas.1111715109.

36. Farovik, A., Place, R.J., McKenzie, S., Porter, B., Munro, C.E., and Eichenbaum, H. (2015). Orbitofrontal cortex encodes memories within value-based schemas and represents contexts that guide memory retrieval. J. Neurosci. *35*, 8333–8344. https://doi.org/10.1523/JNEUROSCI.0134-15.2015.

37. Wikenheiser, A.M., Gardner, M.P.H., Mueller, L.E., and Schoenbaum, G. (2021). Spatial representations in rat orbitofrontal cortex. J. Neurosci. *41*, 6933–6945. https://doi.org/10.1523/JNEUROSCI.0830-21.2021.

38. Banerjee, A., Parente, G., Teutsch, J., Lewis, C., Voigt, F., and Helmchen, F. (2020). Value-guided remapping of sensory circuits by lateral orbitofrontal cortex in reversal learning. Nature *585*, 245–250. https://doi.org/10.1101/2020.03.11.982744.

39. Liu, D., Deng, J., Zhang, Z., Zhang, Z.Y., Sun, Y.G., Yang, T., and Yao, H. (2020). Orbitofrontal control of visual cortex gain promotes visual associative learning. Nat. Commun. *11*, 2784. https://doi.org/10.1038/s41467-020-16609-7.

40. Liu, Y., Xin, Y., and Xu, N.-L. (2021). A cortical circuit mechanism for structural knowledge-based flexible sensorimotor decision-making. Neuron *109*, 2009–2024.e6. https://doi.org/10.1016/j.neuron.2021.04.014.

41. Mittelstadt, J.K., and Kanold, P.O. (2023). Orbitofrontal cortex conveys stimulus and task information to the auditory cortex. Curr. Biol. *33*, 4160–4173.e4. https://doi.org/10.1016/j.cub.2023.08.059.

42. Mast, T.E., and Watson, C.S. (1968). Attention and auditory evoked responses to low-detectability signals. Percept. Psychophys. *4*, 237–240. https://doi.org/10.3758/BF03206309.

43. Niwa, M., O'Connor, K.N., Engall, E., Johnson, J.S., and Sutter, M.L. (2015). Hierarchical effects of task engagement on amplitude modulation encoding in auditory cortex. J. Neurophysiol. *113*, 307–327. https://doi.org/10.1152/jn.00458.2013.

44. Pfingst, B.E., O'Connor, T.A., and Miller, J.M. (1977). Response plasticity of neurons in auditory cortex of the rhesus monkey. Exp. Brain Res. *29*, 393–404. https://doi.org/10.1007/BF00236178.

45. Saderi, D., Schwartz, Z.P., Heller, C.R., Pennington, J.R., and David, S.V. (2021). Dissociation of task engagement and arousal effects in auditory cortex and midbrain. eLife *10*, 21–25. https://doi.org/10.7554/eLife.60153.

46. von Trapp, G., Buran, B.N., Sen, K., Semple, M.N., and Sanes, D.H. (2016). A decline in response variability improves neural signal detection during auditory task performance. J. Neurosci. *36*, 11097–11106. https://doi.org/10.1523/JNEUROSCI.1302-16.2016.

47. Kuchibhotla, K.V., Gill, J.V., Lindsay, G.W., Papadoyannis, E.S., Field, R.E., Sten, T.A.H., Miller, K.D., and Froemke, R.C. (2017). Parallel processing by cortical inhibition enables context-dependent behavior. Nat. Neurosci. *20*, 62–71. https://doi.org/10.1038/nn.4436.

48. Atiani, S., Elhilali, M., David, S.V., Fritz, J.B., and Shamma, S.A. (2009). Task difficulty and performance induce diverse adaptive patterns in gain and shape of primary auditory cortical receptive fields. Neuron *61*, 467–480. https://doi.org/10.1016/j.neuron.2008.12.027.

49. Cohen, J.Y., Haesler, S., Vong, L., Lowell, B.B., and Uchida, N. (2012). Neuron-type-specific signals for reward and punishment in the ventral tegmental area. Nature *482*, 85–88. https://doi.org/10.1038/nature10754.

50. Rudebeck, P.H., and Murray, E.A. (2014). The orbitofrontal oracle: cortical mechanisms for the prediction and evaluation of specific behavioral outcomes. Neuron *84*, 1143–1156. https://doi.org/10.1016/j.neuron.2014.10.049.

51. Torregrossa, M.M., Quinn, J.J., and Taylor, J.R. (2008). Impulsivity, compulsivity, and habit: the role of orbitofrontal cortex revisited. Biol. Psychiatry *63*, 253–255. https://doi.org/10.1016/j.biopsych.2007.11.014.

52. Winstanley, C.A., Theobald, D.E.H., Cardinal, R.N., and Robbins, T.W. (2004). Contrasting roles of basolateral amygdala and orbitofrontal cortex in impulsive choice. J. Neurosci. *24*, 4718–4722. https://doi.org/10.1523/JNEUROSCI.5606-03.2004.

53. Caras, M.L., and Sanes, D.H. (2019). Neural variability limits adolescent skill learning. J. Neurosci. *39*, 2889–2902. https://doi.org/10.1523/JNEUROSCI.2878-18.2019.

54. Yin, P., Johnson, J.S., O'Connor, K.N., and Sutter, M.L. (2011). Coding of amplitude modulation in primary auditory cortex. J. Neurophysiol. *105*, 582–600. https://doi.org/10.1152/jn.00621.2010.

55. Glennon, E., Carcea, I., Martins, A.R.O., Multani, J., Shehu, I., Svirsky, M.A., and Froemke, R.C. (2019). Locus coeruleus activation accelerates perceptual learning. Brain Res. *1709*, 39–49. https://doi.org/10.1016/j.brainres.2018.05.048.

56. Marlin, B.J., Mitre, M., D'amour, J.A., Chao, M.V., and Froemke, R.C. (2015). Oxytocin enables maternal behaviour by balancing cortical inhibition. Nature *520*, 499–504. https://doi.org/10.1038/nature14402.

57. Schroeder, A., Pardi, M.B., Keijser, J., Dalmay, T., Groisman, A.I., Schuman, E.M., Sprekeler, H., and Letzkus, J.J. (2023). Inhibitory top-down projections from zona incerta mediate neocortical memory. Neuron *111*, 727–738.e8. https://doi.org/10.1016/j.neuron.2022.12.010.

58. Winkowski, D.E., Nagode, D.A., Donaldson, K.J., Yin, P., Shamma, S.A., Fritz, J.B., and Kanold, P.O. (2018). Orbitofrontal cortex neurons respond

to sound and activate primary auditory cortex neurons. Cereb. Cortex *28*, 868–879. https://doi.org/10.1093/cercor/bhw409.

59. Froemke, R.C., Merzenich, M.M., and Schreiner, C.E. (2007). A synaptic memory trace for cortical receptive field plasticity. Nature *450*, 425–429. https://doi.org/10.1038/nature06289.
60. Letzkus, J.J., Wolff, S.B.E., Meyer, E.M.M., Tovote, P., Courtin, J., Herry, C., and Lüthi, A. (2011). A disinhibitory microcircuit for associative fear learning in the auditory cortex. Nature *480*, 331–335. https://doi.org/10.1038/nature10674.
61. Froemke, R.C., Carcea, I., Barker, A.J., Yuan, K., Seybold, B.A., Martins, A.R.O., Zaika, N., Bernstein, H., Wachs, M., Levis, P.A., et al. (2013). Long-term modification of cortical synapses improves sensory perception. Nat. Neurosci. *16*, 79–88. https://doi.org/10.1038/nn.3274.
62. Guo, W., Robert, B., and Polley, D.B. (2019). The cholinergic basal forebrain links auditory stimuli with delayed reinforcement to support learning. Neuron *103*, 1164–1177.e6. https://doi.org/10.1016/j.neuron.2019.06.024.
63. Miasnikov, A.A., Chen, J.C., and Weinberger, N.M. (2006). Rapid induction of specific associative behavioral memory by stimulation of the nucleus basalis in the rat. Neurobiol. Learn. Mem. *86*, 47–65. https://doi.org/10.1016/j.nlm.2005.12.010.
64. Miasnikov, A.A., Chen, J.C., and Weinberger, N.M. (2008). Specific auditory memory induced by nucleus basalis stimulation depends on intrinsic acetylcholine. Neurobiol. Learn. Mem. *90*, 443–454. https://doi.org/10.1016/j.nlm.2008.05.010.
65. Aston-Jones, G., Rajkowski, J., and Kubiak, P. (1997). Conditioned responses of monkey locus coeruleus neurons anticipate acquisition of discriminative behavior in a vigilance task. Neuroscience *80*, 697–715. https://doi.org/10.1016/S0306-4522(97)00060-2.
66. Bao, S., Chan, V.T., and Merzenich, M.M. (2001). Cortical remodelling induced by activity of ventral tegmental dopamine neurons. Nature *412*, 79–83. https://doi.org/10.1038/35083586.
67. Brunk, M.G.K., Deane, K.E., Kisse, M., Deliano, M., Vieweg, S., Ohl, F.W., Lippert, M.T., and Happel, M.F.K. (2019). Optogenetic stimulation of the VTA modulates a frequency-specific gain of thalamocortical inputs in infragranular layers of the auditory cortex. Sci. Rep. *9*, 20385. https://doi.org/10.1038/s41598-019-56926-6.
68. Happel, M.F.K., Deliano, M., Handschuh, J., and Ohl, F.W. (2014). Dopamine-modulated recurrent corticoefferent feedback in primary sensory cortex promotes detection of behaviorally relevant stimuli. J. Neurosci. *34*, 1234–1247. https://doi.org/10.1523/JNEUROSCI.1990-13.2014.
69. Stark, H., and Scheich, H. (1997). Dopaminergic and serotonergic neurotransmission systems are differentially involved in auditory cortex learning: a long-term microdialysis study of metabolites. J. Neurochem. *68*, 691–697. https://doi.org/10.1046/j.1471-4159.1997.68020691.x.
70. Martins, A.R.O., and Froemke, R.C. (2015). Coordinated forms of noradrenergic plasticity in the locus coeruleus and primary auditory cortex. Nat. Neurosci. *18*, 1483–1492. https://doi.org/10.1038/nn.4090.
71. Edeline, J.-M., Manunta, Y., and Hennevin, E. (2011). Induction of selective plasticity in the frequency tuning of auditory cortex and auditory thalamus neurons by locus coeruleus stimulation. Hear. Res. *274*, 75–84. https://doi.org/10.1016/j.heares.2010.08.005.
72. Russchen, F.T., Amaral, D.G., and Price, J.L. (1985). The afferent connections of the substantia innominata in the monkey, Macaca fascicularis. J. Comp. Neurol. *242*, 1–27. https://doi.org/10.1002/cne.902420102.
73. Aston-Jones, G., and Cohen, J.D. (2005). Adaptive gain and the role of the locus coeruleus–norepinephrine system in optimal performance. J. Comp. Neurol. *493*, 99–110. https://doi.org/10.1002/cne.20723.
74. Watabe-Uchida, M., Zhu, L., Ogawa, S.K., Vamanrao, A., and Uchida, N. (2012). Whole-brain mapping of direct inputs to midbrain dopamine neurons. Neuron *74*, 858–873. https://doi.org/10.1016/j.neuron.2012.03.017.
75. Jo, Y.S., and Mizumori, S.J.Y. (2016). Prefrontal regulation of neuronal activity in the ventral tegmental area. Cereb. Cortex *26*, 4057–4068. https://doi.org/10.1093/cercor/bhv215.
76. Douglas, R.J., Koch, C., Mahowald, M., Martin, K.A.C., and Suarez, H.H. (1995). Recurrent excitation in neocortical circuits. Science *269*, 981–985. https://doi.org/10.1126/science.7638624.
77. Harris, K.D., and Mrsic-Flogel, T.D. (2013). Cortical connectivity and sensory coding. Nature *503*, 51–58. https://doi.org/10.1038/nature12654.
78. Stalnaker, T.A., Cooch, N.K., and Schoenbaum, G. (2015). What the orbitofrontal cortex does not do. Nat. Neurosci. *18*, 620–627. https://doi.org/10.1038/nn.3982.
79. Walton, M.E., Behrens, T.E.J., Buckley, M.J., Rudebeck, P.H., and Rushworth, M.F.S. (2010). Separable learning systems in the macaque brain and the role of orbitofrontal cortex in contingent learning. Neuron *65*, 927–939. https://doi.org/10.1016/j.neuron.2010.02.027.
80. Costa, K.M., Scholz, R., Lloyd, K., Moreno-Castilla, P., Gardner, M.P.H., Dayan, P., and Schoenbaum, G. (2023). The role of the lateral orbitofrontal cortex in creating cognitive maps. Nat. Neurosci. *26*, 107–115. https://doi.org/10.1038/s41593-022-01216-0.
81. Sarlitto, M.C., Foilb, A.R., and Christianson, J.P. (2018). Inactivation of the ventrolateral orbitofrontal cortex impairs flexible use of safety signals. Neuroscience *379*, 350–358. https://doi.org/10.1016/j.neuroscience.2018.03.037.
82. Takahashi, Y.K., Roesch, M.R., Stalnaker, T.A., Haney, R.Z., Calu, D.J., Taylor, A.R., Burke, K.A., and Schoenbaum, G. (2009). The orbitofrontal cortex and ventral tegmental area are necessary for learning from unexpected outcomes. Neuron *62*, 269–280. https://doi.org/10.1016/j.neuron.2009.03.005.
83. Hartikainen, K.M., Ogawa, K.H., and Knight, R.T. (2012). Orbitofrontal cortex biases attention to emotional events. J. Clin. Exp. Neuropsychol. *34*, 588–597. https://doi.org/10.1080/13803395.2012.666231.
84. Xie, Y., Nie, C., and Yang, T. (2018). Covert shift of attention modulates the value encoding in the orbitofrontal cortex. eLife *7*, e31507. https://doi.org/10.7554/eLife.31507.
85. Chase, E.A., Tait, D.S., and Brown, V.J. (2012). Lesions of the orbital prefrontal cortex impair the formation of attentional set in rats. Eur. J. Neurosci. *36*, 2368–2375. https://doi.org/10.1111/j.1460-9568.2012.08141.x.
86. McAlonan, K., and Brown, V.J. (2003). Orbital prefrontal cortex mediates reversal learning and not attentional set shifting in the rat. Behav. Brain Res. *146*, 97–103. https://doi.org/10.1016/j.bbr.2003.09.019.
87. Gallagher, M., McMahan, R.W., and Schoenbaum, G. (1999). Orbitofrontal cortex and representation of incentive value in associative learning. J. Neurosci. *19*, 6610–6614. https://doi.org/10.1523/JNEUROSCI.19-15-06610.1999.
88. Schoenbaum, G., Setlow, B., Nugent, S.L., Saddoris, M.P., and Gallagher, M. (2003). Lesions of orbitofrontal cortex and basolateral amygdala complex disrupt acquisition of odor-guided discriminations and reversals. Learn. Mem. *10*, 129–140. https://doi.org/10.1101/lm.55203.
89. Izquierdo, A., Suda, R.K., and Murray, E.A. (2004). Bilateral orbital prefrontal cortex lesions in rhesus monkeys disrupt choices guided by both reward value and reward contingency. J. Neurosci. *24*, 7540–7548. https://doi.org/10.1523/JNEUROSCI.1921-04.2004.
90. Ostlund, S.B., and Balleine, B.W. (2007). Orbitofrontal cortex mediates outcome encoding in Pavlovian but not instrumental conditioning. J. Neurosci. *27*, 4819–4825. https://doi.org/10.1523/JNEUROSCI.5443-06.2007.
91. Schoenbaum, G., Roesch, M.R., Stalnaker, T.A., and Takahashi, Y.K. (2009). A new perspective on the role of the orbitofrontal cortex in adaptive behaviour. Nat. Rev. Neurosci. *10*, 885–892. https://doi.org/10.1038/nrn2753.

92. Barbosa, J., Proville, R., Rodgers, C.C., DeWeese, M.R., Ostojic, S., and Boubenec, Y. (2023). Early selection of task-relevant features through population gating. Nat. Commun. *14*, 6837. https://doi.org/10.1038/s41467-023-42519-5.

93. Casado-Román, L., Carbajal, G.V., Pérez-González, D., and Malmierca, M.S. (2020). Prediction error signaling explains neuronal mismatch responses in the medial prefrontal cortex. PLoS Biol. *18*, e3001019. https://doi.org/10.1371/journal.pbio.3001019.

94. Little, D.F., Cheng, H.H., and Wright, B.A. (2019). Inducing musical-interval learning by combining task practice with periods of stimulus exposure alone. Atten. Percept. Psychophys. *81*, 344–357. https://doi.org/10.3758/s13414-018-1584-x.

95. Seitz, A.R., and Dinse, H.R. (2007). A common framework for perceptual learning. Curr. Opin. Neurobiol. *17*, 148–153. https://doi.org/10.1016/j.conb.2007.02.004.

96. Wright, B.A., Sabin, A.T., Zhang, Y., Marrone, N., and Fitzgerald, M.B. (2010). Enhancing perceptual learning by combining practice with periods of additional sensory stimulation. J. Neurosci. *30*, 12868–12877. https://doi.org/10.1523/JNEUROSCI.0487-10.2010.

97. Pachitariu, M., Sridhar, S., Pennington, J., and Stringer, C. (2024). Spike sorting with Kilosort4. Nat. Methods *21*, 914–921. https://doi.org/10.1038/s41592-024-02232-7.

98. Schneider, C.A., Rasband, W.S., and Eliceiri, K.W. (2012). NIH Image to ImageJ: 25 years of image analysis. Nat. Methods *9*, 671–675. https://doi.org/10.1038/nmeth.2089.

99. Caras, M.L., and Sanes, D.H. (2015). Sustained perceptual deficits from transient sensory deprivation. J. Neurosci. *35*, 10831–10842. https://doi.org/10.1523/JNEUROSCI.0837-15.2015.

100. Sarro, E.C., Von Trapp, G., Mowery, T.M., Kotak, V.C., and Sanes, D.H. (2015). Cortical synaptic inhibition declines during auditory learning. J. Neurosci. *35*, 6318–6325. https://doi.org/10.1523/JNEUROSCI.4051-14.2015.

101. Sarro, E.C., and Sanes, D.H. (2010). Prolonged maturation of auditory perception and learning in gerbils. Dev. Neurobiol. *70*, 636–648. https://doi.org/10.1002/dneu.20801.

102. Sarro, E.C., and Sanes, D.H. (2011). The cost and benefit of juvenile training on adult perceptual skill. J. Neurosci. *31*, 5383–5391. https://doi.org/10.1523/JNEUROSCI.6137-10.2011.

103. Anbuhl, K.L., Yao, J.D., Hotz, R.A., Mowery, T.M., and Sanes, D.H. (2022). Auditory processing remains sensitive to environmental experience during adolescence in a rodent model. Nat. Commun. *13*, 2872. https://doi.org/10.1038/s41467-022-30455-9.

104. Mowery, T.M., Caras, M.L., Hassan, S.I., Wang, D.J., Dimidschstein, J., Fishell, G., and Sanes, D.H. (2019). Preserving inhibition during developmental hearing loss rescues auditory learning and perception. J. Neurosci. *39*, 8347–8361. https://doi.org/10.1523/JNEUROSCI.0749-19.2019.

105. Rosen, M.J., Sarro, E.C., Kelly, J.B., and Sanes, D.H. (2012). Diminished behavioral and neural sensitivity to sound modulation is associated with moderate developmental hearing loss. PLoS One *7*, e41514. https://doi.org/10.1371/journal.pone.0041514.

106. Ying, R., Stolzberg, D.J., and Caras, M.L. (2024). Neural correlates of flexible sound perception in the auditory midbrain and thalamus. Preprint at bioRxiv. https://doi.org/10.1101/2024.04.12.589266.

107. Viemeister, N.F. (1979). Temporal modulation transfer functions based upon modulation thresholds. J. Acoust. Soc. Am. *66*, 1364–1380. https://doi.org/10.1121/1.383531.

108. Radtke-Schuller, S., Schuller, G., Angenstein, F., Grosser, O.S., Goldschmidt, J., and Budinger, E. (2016). Brain atlas of the Mongolian gerbil (Meriones unguiculatus) in CT/MRI-aided stereotaxic coordinates. Brain Struct. Funct. *221*, 1–272. https://doi.org/10.1007/s00429-016-1259-0.

109. Siegle, J.H., López, A.C., Patel, Y.A., Abramov, K., Ohayon, S., and Voigts, J. (2017). Open Ephys: an open-source, plugin-based platform for multichannel electrophysiology. J. Neural Eng. *14*, 045003. https://doi.org/10.1088/1741-2552/aa5eea.

110. Hill, D.N., Mehta, S.B., and Kleinfeld, D. (2011). Quality metrics to accompany spike sorting of extracellular signals. J. Neurosci. *31*, 8699–8705. https://doi.org/10.1523/JNEUROSCI.0971-11.2011.

111. Zhang, Y., Rózsa, M., Liang, Y., Bushey, D., Wei, Z., Zheng, J., Reep, D., Broussard, G.J., Tsang, A., Tsegaye, G., et al. (2023). Fast and sensitive GCaMP calcium indicators for imaging neural populations. Nature *615*, 884–891. https://doi.org/10.1038/s41586-023-05828-9.

112. Kim, C.K., Yang, S.J., Pichamoorthy, N., Young, N.P., Kauvar, I., Jennings, J.H., Lerner, T.N., Berndt, A., Lee, S.Y., Ramakrishnan, C., et al. (2016). Simultaneous fast measurement of circuit dynamics at multiple sites across the mammalian brain. Nat. Methods *13*, 325–328. https://doi.org/10.1038/nmeth.3770.

113. Martianova, E., Aronson, S., and Proulx, C.D. (2019). Multi-fiber photometry to record neural activity in freely-moving animals. J. Vis. Exp. 1–9. https://doi.org/10.3791/60278.

114. Zhang, Z.M., Chen, S., and Liang, Y.Z. (2010). Baseline correction using adaptive iteratively reweighted penalized least squares. Analyst *135*, 1138–1146. https://doi.org/10.1039/b922045c.

115. Brooks, M.E., Kristensen, K., van Benthem, K.J., Magnusson, A., Berg, C.W., Nielsen, A., Skaug, H.J., Mächler, M., and Bolker, B.M. (2017). glmmTMB balances speed and flexibility among packages for zero-inflated generalized linear mixed modeling. R J. *9*, 378–400. https://doi.org/10.32614/RJ-2017-066.

116. John, F., and Weisberg, S. (2019). An R Companion to Applied Regression, Third Edition (Sage Publications).

117. Hartig, F. (2021). DHARMa: residual diagnostics for hierarchical (multi-level/mixed) regression models. Version R package version 0.4.3.

118. Bliss, C.I., Greenwood, M.L., and White, E.S. (1956). A rankit analysis of paired comparisons for measuring the effect of sprays on flavor. Biometrics *12*, 381. https://doi.org/10.2307/3001679.

STAR★METHODS

KEY RESOURCES TABLE

REAGENT or RESOURCE	SOURCE	IDENTIFIER
Antibodies		
Rabbit polyclonal anti-GFP	Invitrogen	#A11122; RRID: AB_221569
Goat anti-rabbit Alexa-488	Invitrogen	#A32731; RRID: AB_2633280
Bacterial and virus strains		
AAVrg-syn-jGCaMP8s-WPRE	Addgene	162374-AAVrg; RRID: Addgene_162374
Chemicals, peptides, and recombinant proteins		
FluoSpheres (0.2 μm)	Invitrogen	F-8848
FluoroRuby	Molecular Probes	D1817
Muscimol	Abcam	ab120094
Deposited data		
Electrophysiology, photometry, and behavioral data	Digital Repository at the University of Maryland	UMD DRUM Data: https://doi.org/10.13016/qzzx-zfuh
Experimental models: Organisms/strains		
Gerbil (Meriones unguiculatus)	Charles River Laboratories	https://criver.com/
Software and algorithms		
Behavioral control software	ePsych (Dr. Daniel Stolzberg)	https://github.com/caraslab/epsych
Electrophysiology processing	Custom code; Kilosort 2[97]; Phy	https://github.com/caraslab/caraslab-spikesortingKS2; https://github.com/caraslab/Caraslab_EPhys_preprocessing_pipeline; https://github.com/cortex-lab/phy
Photometry processing	Custom code	www.github.com/caraslab/caraslab-fiberphotometry; https://github.com/caraslab/Caraslab_FP_preprocessing_pipeline
Behavioral data processing	Custom code	www.github.com/caraslab/caraslab-behavior-analysis
Data analysis and statistics	Custom code	www.github.com/caraslab/MacedoLima_CurBiol2024
ImageJ	Schneider et al.[98]	www.imagej.nih.gov/ij
PyCharm	JetBrains	www.jetbrains.com
RStudio	Posit	www.posit.co
MatLab	MathWorks	www.mathworks.com
Adobe Illustrator 2024	Adobe	www.adobe.com

RESOURCE AVAILABILITY

Lead contact

Further information and requests for resources and reagents should be directed to and will be fulfilled by the lead contact, Melissa L. Caras (mcaras@umd.edu).

Materials availability

This study did not generate new unique reagents.

Data and code availability

All data reported in this paper has been deposited in the Digital Repository at the University of Maryland (UMD DRUM Data: https://doi.org/10.13016/qzzx-zfuh). All relevant MATLAB, Python and R code for processing behavioral and physiology data are available at https://github.com/caraslab. Data analysis, plotting and statistics supporting code is available at https://github.com/caraslab/MacedoLima_CurBiol2024.

EXPERIMENTAL MODEL AND SUBJECT DETAILS

Subjects

Adult Mongolian gerbils (*Meriones unguiculatus*; n = 25, 13 females) used in this study were bred in-house from commercially obtained breeding pairs (Charles River). Animals were kept under a 12 hr light:12 hr dark cycle and on *ad libitum* food, enrichment, and water access until placed on controlled water access for behavioral experiments. All procedures were approved by the Institutional Animal Care and Use Committee at the University of Maryland College Park.

METHOD DETAILS

Choice of behavioral task

Auditory perception was tested with an aversive go/no-go AM detection task as previously described.[99–102] We chose to use this approach for several reasons. First, it is easy to quickly train animals on the task. Naïve to expert performance is typically reached within 1-2 weeks. Second, it offers superb behavioral control. Expert animals commonly exhibit extremely low false alarm rates and high hit rates, resulting in high-quality, interpretable data. Third, it has been used extensively (by our group and others) to evaluate behavioral AM sensitivity in the Mongolian gerbil.[13,53,99–105] Finally, it elicits robust and reliable context-dependent modulations of neural activity in the auditory midbrain, thalamus, and cortex.[13,106] We therefore had clear, testable predictions and an extremely solid basis for comparison when designing the current experiments.

Behavioral set up

A custom test cage (CCMI Plastics) containing a stainless-steel water spout and metal floor plate was positioned inside a sound attenuating booth (GretchKen). Infrared detection of the animal at the spout triggered water delivery via a programmable syringe pump (NE-1000, New Era Pump Systems). Sound stimuli were delivered via a calibrated free-field speaker (DX25TG59-04 1″ Fabric Dome Tweeter, Peerless by Tymphany) positioned directly above the test cage. Shocks were delivered by an H13–15 Precision Animal Shocker (Colburn). Behavior was monitored remotely via webcam. Data acquisition, sound delivery, and digital outputs were controlled via an RZ6 multifunction processor (Tucker Davis Technologies, TDT).

Behavioral training and testing

During an initial procedural training stage, animals were placed on controlled water access and learned to drink steadily from a spout while in the presence of a ''safe cue'' (unmodulated broadband noise, 0.1-20 kHz, 45 dB SPL). Animals were then trained to withdraw from the spout when the sound changed to the ''warn'' cue (5 Hz sinusoidal amplitude modulated (AM) noise, 0 dB re: 100% depth, 1 second duration) by pairing the warn cue with a mild shock (0.5-1 mA, 300 msec). Warn trials were randomly interspersed with 3-5 safe trials, but only while animals made contact with the spout. The gain of the AM signal was adjusted to control for changes in average power.[107]

The animal's contact with the spout was monitored during the final 100 msec of each trial. Breaking spout contact for at least 50 msec during the monitoring window was considered a spout 'withdrawal,' and was scored as a 'hit' on AM trials and as a 'false alarm' on non-AM trials. Behavioral performance was assessed by $d' = z(HR) - z(FAR)$, where z(HR) and z(FAR) are the z-scores of the hit rates (HR) and false alarm rates (FAR), respectively. To avoid values that approach infinity, extreme HR and FAR values were set to a floor of 5% and a ceiling 95%. Behavioral testing commenced only after an animal achieved a d' >= 2 in a single session.

For passive sound exposure sessions, animals were placed in the test cage but did not have access to a waterspout. All other elements of the experimental apparatus were identical to the detection task. Sounds were presented in a manner similar to that of the task (AM stimuli randomly interspersed with 3-5 seconds of unmodulated noise).

Note that the fourteen animals used for the OFC electrophysiology and fiber photometry experiments (Figures 2, 3, and S1–S3) were recorded from as they underwent a perceptual learning protocol in which they were trained to detect progressively smaller AM depths. The details of this procedure have been previously described.[13] OFC's involvement in perceptual learning will be explored in a future manuscript.

Electrode implant procedures

NeuroNexus 64-channel probes (OFC: A4x16-Poly2-5mm-20s-lin-160; auditory cortex: Buzsaki64_5x12) were mounted on custom-made microdrives. The backs of the electrode shanks were painted with azide-free fluorescent microspheres (FluoSpheres 0.2 μm; Invitrogen) just before implantation. On the day before surgery, animals were placed on antibiotic treatment (minocycline in drinking water; 0.02 mg/mL) and given meloxicam (1.5 mg/kg). On the day of the surgery, they were given another dose of meloxicam plus dexamethasone (0.35 mg/kg). Then, they were anesthetized with isoflurane (1-5%) and secured in a stereotaxic apparatus (Kopf). Ophthalmic ointment was applied to the eyes and alternating swabs of alcohol and betadine were applied to the skin on the top of the head. The skull was exposed and dried with hydrogen peroxide, three or four bone screws were inserted, and craniotomy locations were marked over left OFC or left auditory cortex after leveling the head. Note that we leveled the animal's head between lambda and bregma, rather than between lambda and the occipital ridge as in the gerbil brain atlas.[108] Therefore, all of our rostro-caudal coordinates differ from those reported in the atlas.

Before an auditory cortex craniotomy, the temporalis muscle insertion was detached, and the muscle was separated from skull using dry SurgiFoam (Ethicon). The skull and screws were covered with C&B Metabond (Parkell) for better implant adhesion. The edges of the craniotomy were thinned by drilling and the bone flap was removed. A durotomy was made over the area of interest and electrodes were implanted using the following coordinates (all relative to lambda). OFC: 1.20–1.50 mm lateral, 9.05–9.50 mm rostral, 2.00–2.50 mm ventral, angle=0° from vertical; implanted along coronal plane. Auditory cortex: 4.80 mm lateral, 3.90 mm rostral (anterior shank), 1.10-1.50 mm ventral, angle=20° clockwise from vertical plane facing the animal's posterior side, implanted along parasagittal plane. A ground wire was inserted into the right caudal hemisphere. Implants were secured with dental cement (Palacos). The day following surgery, animals were given another dose of meloxicam and dexamethasone. Antibiotic treatment continued for an additional six days. Controlled water access and behavioral experiments started at least seven days after surgery.

Electrophysiology

Extracellular recordings from the OFC were obtained from freely-moving animals before (passive-pre), during (task), and after (passive-post) behavioral testing sessions that took place every 24-48 hours. The number of AM stimulus presentations was similar across behavioral contexts (passive-pre:101 ± 0.12; task: 110 ± 3.16; passive-post: 101 ± 0.24 trials; means ± SEMs).

Extracellular recordings from the auditory cortex were obtained before (passive-pre) and during (task) behavioral testing sessions that took place every 24-48 hours. The number of AM stimulus presentations was similar across behavioral contexts (passive-pre: 38.3 ± 8.08; task: 42.5 ±7.05; means ± SEMs).

Neurophysiological signals were obtained via one of two methods: (I) Analog signals were acquired with a 64-channel wireless headstage and receiver (W64, Triangle BioSystems), preamplified and digitized at 24.4 kHz sampling rate (PZ5; Tucker Davis Technologies, TDT), and integrated with behavioral timestamps via RZ2 and RZ6 processors controlled by the Synapse software suite (TDT). Raw signals were sent to an RS4 data streamer (TDT) and stored online. (II) Signals were preamplified and digitized at 30 kHz by a 64-channel RHD headstage (Intan Technologies) connected to a slip-ring commutator (Taidacent; purchased from Amazon) and integrated with behavioral timestamps using an RHD recording controller (Intan) and OpenEphys software.[109]

Offline signals were high-pass filtered at 150 Hz and common-median referenced across channels. Multi- and single-unit sorting was performed using Kilosort2.[97] Recordings under all three behavioral contexts (passive-pre, task, passive-post) always occurred consecutively on the same day within a single 40–60 min window. Therefore, it's reasonable to consider each day's recording as a single session that encompassed three different behavioral contexts, similar to many previously published reports.[13,23,30,48] We therefore concatenated all recordings from the same day together for sorting in a single Kilosort run. This approach allowed us to identify single units that were present during each behavioral context. Sorting results were manually curated using Phy (https://github.com/cortex-lab/phy). Clusters were classified as putative single-units during manual curation when they presented with a high signal-to-noise ratio, clear refractory period gap in the autocorrelogram and clear cross-correlogram isolation from neighboring clusters. After manual curation, the Allen Brain Institute quality metrics 'presence ratio', 'amplitude cutoff fraction missing,' and 'ISI violation false-positive rate' (parameters: isi_threshold = 1.5 ms; min_ISI = 0.15 ms)[110] were calculated (https://allensdk.readthedocs.io/en/latest/_static/examples/nb/ecephys_quality_metrics.html). We also calculated the 'refractory period violation rate' as the percentage of interspike intervals that violated a refractory period of 1.5 msec. Only putative single-units that had a 'presence ratio' > 0.9, 'amplitude cutoff fraction missing' < 0.1, 'ISI violation false-positive rate' < 0.5, and 'refractory period violation rate' < 2% were considered true single-units.

After single- and multi-unit isolation, firing rates were calculated. The window used for calculating firing rates on ''Hit'' trials was the full 1-s AM duration. ''Miss'' trials produced a shock artifact, however. Thus, the window used for calculating firing rates on ''Miss'' trials was the first 950 msec of the AM stimulus. ''False alarm'' trials by definition do not contain an AM period, so we used a 1-s block of non-AM sound during which a false alarm occurred to quantify firing rates. Peristimulus time-histograms (PSTH) were generated using 10-20 msec bins.

Auditory cortical firing rates were transformed to neural d'[13,46] using the formula:

$$d' = \frac{2(\mu FR_{AM} - \mu FR_{NONAM})}{\sigma FR_{AM} + \sigma FR_{NONAM}} \text{(Equation 1)}$$

where μFR_{AM} and μFR_{NONAM} are the mean firing rates and σFR_{AM} and σFR_{NONAM} are the standard deviation of the firing rates during AM and non-AM presentations, respectively. The non-AM period used for these calculations was generally the 1 s non-AM noise period immediately preceding an AM trial. However, if animals withdrew from spout during that period (i.e., false alarm), the nearest previous 1 s period during which the animal did not leave the spout (i.e., correct rejection) was used.

The effect of task engagement on OFC firing rates during non-AM sound presentation was assessed with a Wilcoxon signed-rank test. When $p < 0.05$, the W statistic was used to determine the direction of the change: 'task-enhanced' units exhibited a $W > 0$, while 'task-suppressed' units exhibited $W < 0$. The magnitude of the context modulation was computed for each OFC unit using the z-score formula:

$$\textit{Context modulation} = \frac{\mu FR_{task} - \mu FR_{passive-pre}}{\sqrt{Var(FR_{task}) + Var(FR_{passive-pre})}} \text{(Equation 2)}$$

where μFR_{task} and $\mu FR_{passive-pre}$ are the mean firing rates and $Var(FR_{task})$ and $Var(FR_{passive-pre})$ are the firing rate variances during the task and during the passive-pre periods, respectively.

The response of OFC neurons to AM sound presentation was assessed by calculating the area under the receiver operating characteristic curve (auROC) from peri-stimulus time histograms (PSTH; Figures S1A and S1B), as previously described.[49] This transformation is useful for comparing response dynamics across many units with widely different firing rates. Briefly, PSTHs were generated using 10-ms bins starting 2 s before until 5 s after trial onset (Figure S1A). We compared the histogram of firing rates during a baseline period (from 2 to 1 s before onset) to the histogram during 100-ms windows along the entire PSTH (Figures S1C and S1D). For these comparisons, a moving criterion vector ($\vec{C}$) was created ranging from 0 to maximum firing rate in the PSTH in 100-ms increments. For each value c in $\vec{C}$, we calculated the probability that the activity during each bin was higher than c and plotted it against the probability that the activity during baseline was higher than c, constructing an ROC curve (Figures S1E and S1F). The auROC was calculated via trapezoidal numerical integration. AuROC values range from 0 to 1. Values above 0.5 indicate relative increases, while values below 0.5 indicate relative decreases in firing.

We used auROC responses to assess OFC firing before and after spout withdrawal events (Figures 3 and S1–S3). Because some units increase, while others decrease in firing, we quantified the magnitude of the change, regardless of direction (termed phasic modulation) by subtracting 0.5 from auROC values and taking the absolute value. Phasic modulation values range from 0 (no modulation) to 0.5 (maximum modulation). To examine phasic modulation values prior to spout withdrawal, we focused on the 0.5-s period leading up to a withdrawal on hit and false alarm trials. On miss trials, firing rates were always contaminated by a shock artifact before spout withdrawal; therefore, these trials were not included in this analysis. To examine phasic modulation values after spout withdrawal, we focused on the period between 0.3 and 0.8 s after a withdrawal on hit, miss, and false alarm trials. We used 0.3 s post withdrawal as a starting time to eliminate any remaining shock artifact in miss trials.

Phase-projected vector strength was calculated as in Yin et al.[54] Briefly, the standard trial-by-trial vector strength (VS_t) was calculated as

$$VS_t = \frac{\sqrt{\left(\sum_{i=1}^{n} \cos\theta_i\right)^2 + \left(\sum_{i=1}^{n} \sin\theta_i\right)^2}}{n} \text{(Equation 3)}$$

where n is the number of spikes in a given trial and θ_i is the phase of each spike in relation to the stimulus modulation period. θ_i was calculated as

$$\theta_i = 2\pi \frac{mod(t_i, p)}{p} \text{(Equation 4)}$$

where $mod(t_i, p)$ is the modulo (division remainder) between the spike time relative to the onset of the stimulus t_i and the modulation period for a 5 Hz stimulus p (i.e., 0.2 s). The phase-projected vector strength (VS_{pp}) was calculated as

$$VS_{pp} = VS_t \cos(\varphi_t - \varphi_c) \text{(Equation 5)}$$

where φ_t and φ_c are the trial-by-trial and mean phase angle, calculated as

$$\varphi = \arctan 2 \frac{\sum_{i=1}^{n} \sin\theta_i}{\sum_{i=1}^{n} \cos\theta_i} \text{(Equation 6)}$$

where n is the number of spikes in each trial (φ_t) or in all trials (φ_c), and arctan2(y/x) yields the angle between the x-axis and the vector from [0, 0] to [x, y] (base R function). VS_{pp} ranges from –1 (all spikes in each trial are out of phase with the mean response) to 1 (all spikes are in phase with the mean response).

Fiber photometry

Pre-operative care was as described above. The skull was exposed, dried with hydrogen peroxide, and leveled between lambda and bregma. Two bone screws were inserted, and craniotomy locations were marked over left OFC and left auditory cortex. The temporalis muscle was detached as described above. A virus (AAVrg-syn-jGCaMP8s-WPRE[111]; Addgene) was injected into the left auditory cortex to drive retrograde expression of a genetically-encoded calcium indicator (jGCaMP8s). Injections were made at three locations along the rostro-caudal axis between 2.40 and 3.90 mm rostral to lambda. At each rostro-caudal location, injections were made at two depths relative to the pial surface (0.90 and 0.30 mm; 200 nL per depth), totaling 1200 nL. Each injection was made directly into the temporal aspect of the brain, with the pipette angled 45 degrees laterally. The auditory cortex craniotomy was covered with KwikSil (WPI), and the skin was repositioned to cover the craniotomy. Skin margins were glued with cyanoacrylate tissue adhesive and bone screws and skull were covered with Metabond. Then, a craniotomy over the left OFC was made and an optical fiber (400 μm core; Ø1.25 mm ceramic ferrule; 0.5 NA; RWD Life Science) was implanted in the left OFC using the following coordinates (relative to lambda): 1.2 mm lateral, 8.90–9.05 mm rostral, 2.90–3.20 mm ventral from pial surface). The craniotomy was covered with KwikSil and the fiber was secured with dental cement. Post-operative care was as described above. One control animal (female) was injected with AAVrg-hSyn-eGFP (Addgene) in the left auditory cortex and had a fiber implanted in the left OFC as described above. Controlled water access and behavioral experiments started at least three weeks after surgery to allow for virus expression. Fiber photometry recordings were performed four weeks after surgery.

All optical equipment (patch cords, fluorescence MiniCube, 405 and 465 nm connectorized LEDs, LED driver and Newport photoreceiver module) were purchased from Doric Lenses. LED driver control and photovoltaic signal recording was sampled at 1 kHz using an RZ2 processor and Synapse software (Tucker-Davis Technologies).

Fluorescence was recorded using a 465 nm LED. Calcium-independent (i.e., isosbestic) signals were also recorded using a 405 nm LED to correct for movement artifacts and fluorescence decay. The isosbestic point of GCaMP is ~410 nm.[112]

Before each recording day, patch cords were photobleached overnight. Animal fiber-optic cannulas were connected to the system using a quick-release connector (ADAL3; ThorLabs). Light intensity at the tip of the animal-connecting patch cord was measured with a photodiode power sensor and energy meter (S120C and PM100USB; ThorLabs). Light output (465 and 405 nm respectively) was ~90 and 28 μW for all animals except for one male (~45 and 28 μW).

Photometry signals were processed offline similarly to Martianova et al.[113] Briefly, 465 and 405 nm signals were 5 Hz low-pass filtered and smoothed with a 100-point zero-phase moving average filter. Then, LED onset artifacts were removed, baseline fluctuations were corrected with the adaptive iteratively reweighted Penalized Least Squares algorithm (airPLS)[114] and signals were standardized by median subtraction and division by standard deviation. The standardized 405 signal was fitted to the standardized 465 signal with non-negative robust linear regression and the fit was subtracted from the standardized 465 signal, resulting in a dF/F signal. Finally, this resulting dF/F signal was aligned to behaviorally relevant timestamps and z-scored using a baseline period ranging from 1 s before stimulus until stimulus onset.

Brain cannulation and infusions

Pre- and post-surgical care were as described above. The skull was exposed and dried, and two bone screws were inserted. The skull and screws were covered with C&B Metabond (Parkell) for better implant adhesion. Craniotomies and durotomies were performed over OFC. Double guide cannulas (26-gauge, 5 mm length, 1.5 mm center-to-center distance; PlasticsOne model C235GS-5-1.2/SPC) were inserted just above OFC using the following coordinates (all relative to lambda): lateral = 1.50 mm, rostral = 8.75-9.05 mm, ventral = 1.50 mm; angle=0° from vertical) and secured with dental cement (Palacos). Dummy cannula (33-gauge, 0.25 mm protruding from guide cannula; PlasticsOne model C235DCS-5/SPC) were inserted into the guides and secured in place with a dust cap.

Starting at least seven days after surgery, animals were placed on controlled water access and trained to detect AM sounds as described above. Intracortical infusions only began after animals reached expert performance on the task (d' ≥ 2). Muscimol (abcam) was dissolved in in 0.9% saline to achieve a concentration of 1-2 μg/μL. Aliquots were kept at –20°C and always used within one month of dilution. Infusion cannulas (33 gauge, protruding 1 mm from guide cannula; PlasticsOne model C235IS-5/SPC) containing muscimol or saline were inserted into the guides. Bilateral OFC infusions (0.25-0.5 μL/hemisphere, 0.2 μL/min rate) were made simultaneously via a six-channel programmable pump (NE-1600, New Era) and 10 μL glass syringes (Hamilton 1801). Infusions were performed ~40 min before the behavioral task under light isoflurane anesthesia. The entire infusion procedure lasted between 6 and 10 minutes and animals typically recovered from anesthesia within 2 minutes.

To estimate drug spread and cannula placement, fluororuby (Dextran, Tetramethylrhodamine, 10,000 MW, Lysine Fixable, Invitrogen) was diluted to 5% in sterile saline and infused through the cannulas under light isoflurane anesthesia at the end of the study. Immediately after infusions animals were perfused and brains were processed for histology as described below.

Histology and imaging

At the end of all experiments, animals were deeply anesthetized with a mixture of ketamine (150 mg/kg) and xylazine (6 mg/kg) in sterile saline and transcardially perfused first with ~20 mL of phosphate buffered saline (PBS) then with ~20 mL of 4% paraformaldehyde (PFA) in phosphate buffered saline. After perfusion, implants were removed, and brains were extracted and postfixed in PFA for 1-7 days until sectioning. Brains were then transferred to PBS, embedded in 6% agar, and sectioned on a vibratome (Leica VT-1000S) at 70 μm thickness. Slices were collected and mounted on gelatinized slides and coverslipped with ProLong Gold or Diamond mountant (Molecular Probes).

GFP-containing tissue (photometry experiment) was processed for GFP immunofluorescence for signal amplification. First, free-floating sections were washed in PBS 3x10 min. Non-specific binding was blocked by incubation in 10% normal goat serum (NGS) in phosphate buffered saline containing Triton-X (Sigma; 0.3% PBT) for 2 h at room temperature. Following the blocking step, slices were incubated in 1:1000 rabbit anti-GFP primary antibody (Invitrogen #A11122) diluted in the same blocking solution (NGS + 0.3% PBT) for 1 h at room temperature then 40–48 h at 4°C. Following primary incubation, slices were washed in 0.1% PBT 3x15 min then incubated in 1:1000 goat anti-rabbit Alexa-488 secondary antibody (Invitrogen #A32731) for 1 h at room temperature. Finally, following secondary incubation, slices were washed in 0.1% PBT 3x10 min and coverslipped with ProLong Diamond.

Sections were imaged either via epifluorescence (Leica DM750) or confocal microscopy (Zeiss LSM 980 Airyscan 2) at 10x magnification. For epifluorescence images, tiles were taken manually and stitched together using Photoshop 2023 panorama PhotoMerge function (Adobe). Images were processed using ImageJ.[98]

QUANTIFICATION AND STATISTICAL ANALYSIS

We used the ePsych software developed by Dr. Daniel Stolzberg (https://github.com/dstolz/epsych) for MatLab R2014a (MathWorks) for behavioral data acquisition and control.

All data were processed offline by custom MatLab pipelines (https://github.com/caraslab/caraslab-behavior-analysis, https://github.com/caraslab/caraslab-spikesortingKS2, and https://github.com/caraslab/caraslab-fiberphotometry), then further analyzed by custom Python (https://github.com/caraslab/Caraslab_FP_preprocessing_pipeline and https://github.com/caraslab/Caraslab_EPhys_preprocessing_pipeline) and R routines (https://github.com/caraslab/MacedoLima_CurBiol2024).

Statistical analyses were performed using R (version 4.3.1) and RStudio (version 2023.9.1.494; Posit Software). All statistical results can be found in Tables 1 and S1. Boxplots center lines represent medians, boxes represent 25-75% interquartile range and whiskers represent 10-90% interquartile ranges. Analyses were performed by generalized linear models followed by ANOVA (GLM/ANOVA) using the 'glmmTMB'[115] and the 'car'[116] packages for R. Normality of GLM residuals was assessed after each fit by visually inspecting the distribution of studentized residuals (q-q plots) using the 'DHARMa' package for R.[117] When normality was not fulfilled, data were square-root-, log-, or 'rankit'-transformed,[118] and GLMs were rerun. Before transformation, data containing negative numbers were rescaled using the formula $F(x) = x + 2\left|min\ (\overrightarrow{X})\right|$, where x represents an individual value and $min\ (\overrightarrow{X})$ represents the lowest value in the dataset. When interactions were significant, Bonferroni multiple comparison post-hoc tests using the package 'emmeans' for R (https://github.com/rvlenth/emmeans) were used after ''regridding'' the data into original units if a transformation was required.

All GLM fixed effects can be found in the statistical tables. To test for an effect of behavioral context on OFC activity, we included *Unit* nested under *Subject* (Figure 2F), or *Context* (passive-pre, task, passive-post) nested under *Unit* nested under *Subject* as random effects (Figure 2G). To test for an effect of trial type on phasic modulation, we included *Trial type* nested under *Unit* nested under *Subject* as random effects (Figures 3, S2, and S3). To test for an effect of OFC suppression on behavior, we included *Subject* as a random effect (Figures 4C–4H, 5C, S4, and S5). To test for an effect of behavioral context on auditory cortical activity, we performed separate analyses for each drug treatment (saline or muscimol) and included *Context* (passive, task) nested under *Unit* nested under *Subject* as random effects (Figures 5E–5H and S6), or *Unit* nested under either *Behavioral d'* (Figure 6B) or performance (good vs poor, Figure 6C) nested under Subject as random effects.

Current Biology, Volume *34*

Supplemental Information

Orbitofrontal cortex modulates auditory cortical sensitivity and sound perception in Mongolian gerbils

Matheus Macedo-Lima, Lashaka Sierra Hamlette, and Melissa L. Caras

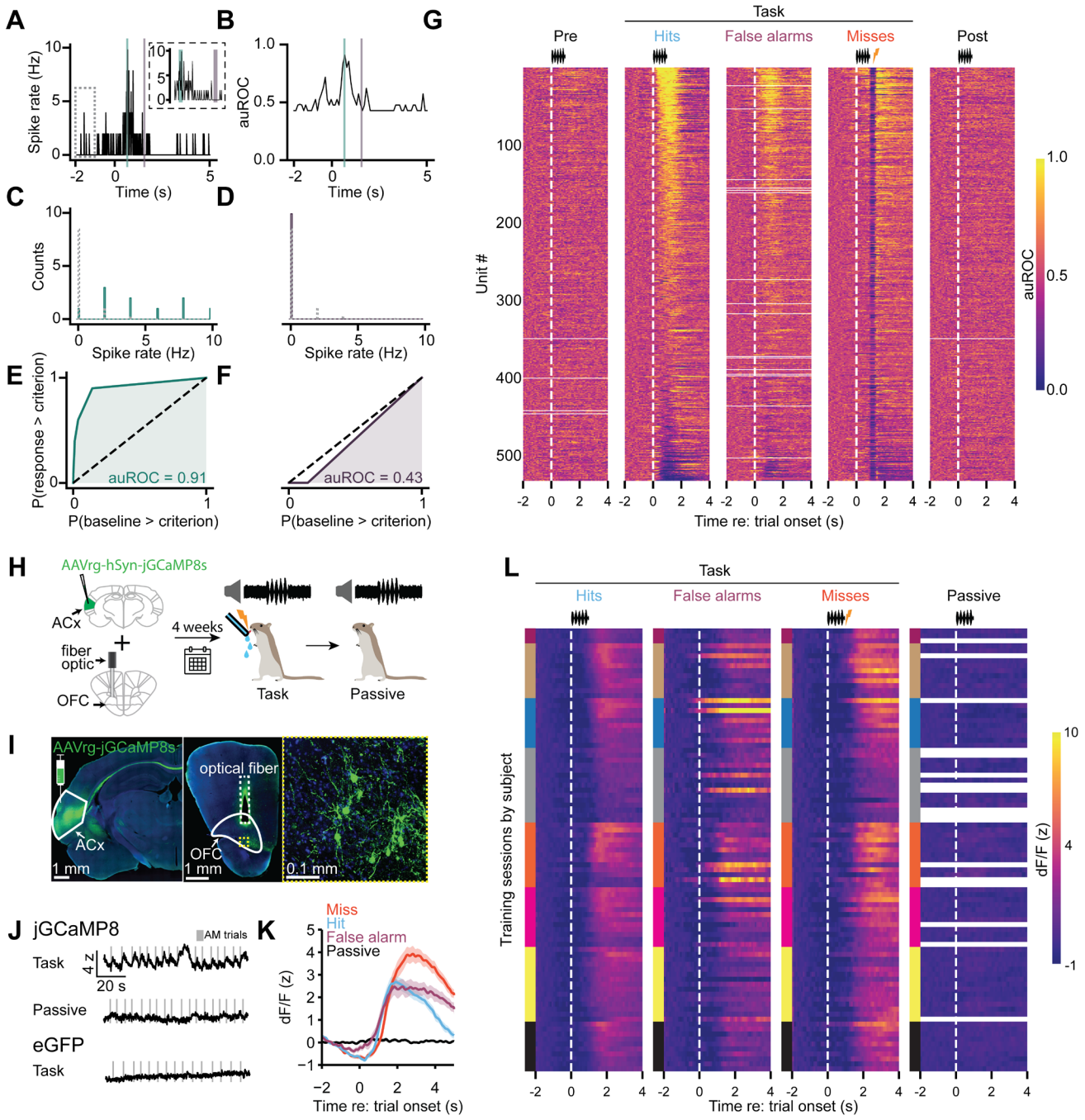

Figure S1. OFC neurons exhibit heterogeneous firing rate changes during sound-guided behavior. Related to Figure 2. (**A-B**) Peri-stimulus time histograms (PSTH) around trials (**A**) were used to generate normalized firing auROC PSTHs (**B**). We compared the spike rate during a baseline period (dashed gray box) to the spike rate during 100-ms windows along the entire PSTH. Two example windows are shown in green and purple. Inset in A represents a magnified view around the windows to illustrate that each 100-ms window contains 10x10-ms spike rate values. (**C-D**) Count histograms illustrating the spike rate bins during baseline period (dashed lines) and during the 100-ms example windows (green and purple solid lines) from the PSTH illustrated in A. Spike rate distributions were compared using a criterion vector (see Supplementary Methods for details) constructing ROCs (**E-F**), from which auROCs could be calculated. (**G**) Heatmaps illustrate normalized neuronal firing (auROC) aligned to trial onset (Time = 0 s; vertical dashed white lines). During passive sound exposure sessions, “trial onset” was defined

as the start of the AM sound. Each row represents one unit and those are ordered by the mean auROC between 0 and 1.5 s during Hit trials, and the same order is used across other trial types. False alarm trials by definition do not contain an AM period, so Time = 0 s represents the onset of a 1-s trial block within which false alarms occurred. Data are from 313 single- and 234 multi-units. Solid white rows are from sessions during which auROC could not be calculated due to an absence of spikes. (**H-L**) OFC neurons that innervate auditory cortex also show increased trial-based activity during task performance. (**H**) Calcium transients from OFC neurons that project to the auditory cortex were recorded via fiber photometry in eight animals (three females). Auditory cortex was injected with a virus to drive the retrograde expression of jGCaMP8s and an optical fiber was implanted in left OFC. After four weeks to allow for virus expression, animals were placed on controlled water access and tested on the AM detection task. Photometry signals were collected during the task and during a period of passive sound exposure immediately following the task. (**I**) Representative images from one animal depicting the virus injection site in auditory cortex (left), fiber location in OFC (middle), and labeled OFC cell bodies (right). (**J**) Calcium transients time-locked to AM trials were only evident during task engagement (top) and not during passive sound exposure (middle). To confirm that the recorded signals were not related to movement artifacts, one female was injected with a virus to drive retrograde expression of enhanced green fluorescent protein (eGFP) and an optical fiber was placed in OFC. No task-related transients were detected in this animal (bottom). (**K**) Mean ± standard error calcium transients from all animals and recording sessions demonstrating strong calcium dynamics around behavioral responses and not during passive AM presentation. (**L**) Heatmaps illustrate calcium dynamics around AM presentations during task and passive periods. Responses were aligned to trial onset (Time = 0 s; vertical dashed white lines). For false alarm trials, Time = 0 s represents the onset of a 1-s trial block within which the false alarm occurred. During passive sound exposure sessions, “trial onset” was defined as the start of the AM sound. Each row represents one session. Vertical color bars to the left of each heatmap indicate sessions from the same animal. Since calcium transients were not evident during passive sound playback, recordings were not performed for every session. Blank rows in the passive session columns represent sessions in which no passive recording was made.

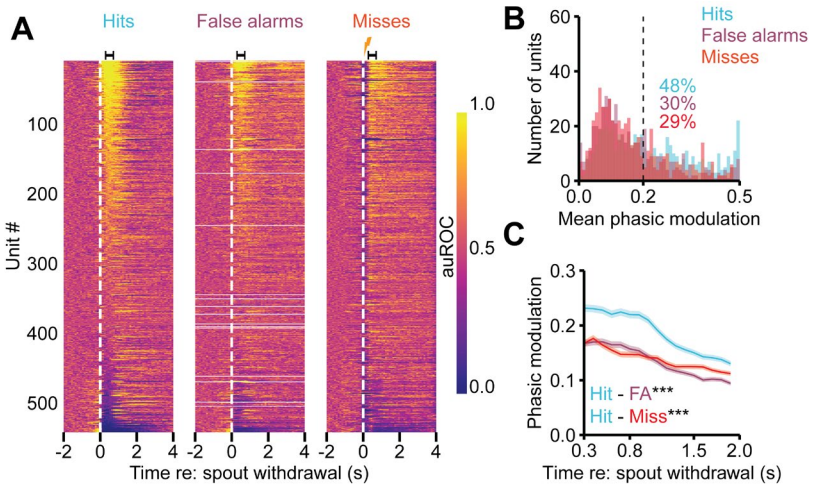

Figure S2. OFC units are sensitive to trial outcome. Related to Figure 3 and Table S1. (**A**) Heatmaps illustrate normalized neuronal firing (auROC) aligned to spout withdrawal (Time = 0 s; vertical dashed white lines). Same data as in Figure 3 but ordered by the mean auROC between 0.3 and 0.8 s post withdrawal (brackets on top of heatmaps) during hit trials. The same order is used for false alarm and miss trials. Values between 0 and 0.3 s were not analyzed because of the shock artifact during miss trials. Solid white rows are from sessions during which auROC could not be calculated due to the absence of spikes. (**B**) Histograms illustrate the distribution of mean phasic modulation between 0.3 and 0.8 s after spout withdrawal during hits, false alarms and misses. Phasic modulation values were calculated as |auROC - 0.5|. Values range from 0 (no modulation) to 0.5 (maximum modulation). Units were classified as significantly modulated if mean phasic modulation was above the 95% confidence interval of the distribution (dashed line). Percentages indicate the proportion of units with significant phasic modulation. (**C**) Mean phasic modulation values 0.3-0.8 s after spout withdrawal (illustrated as mean ± standard error across units) are larger on hit trials than on miss or false alarm trials. ***p < 0.001.

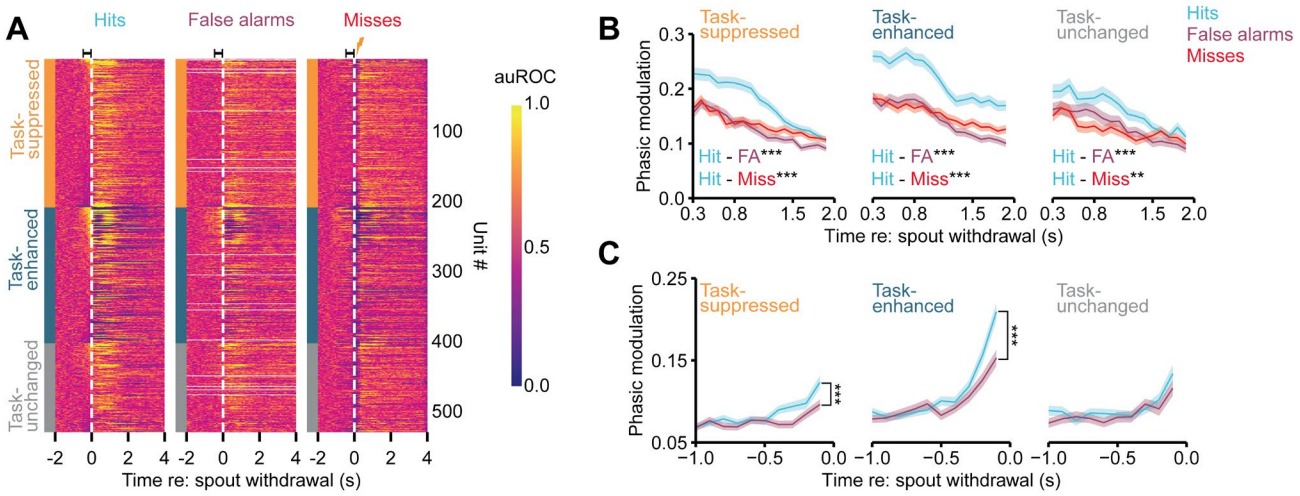

Figure S3. Phasic modulation profile of OFC units separated by tonic firing category. Related to Figure 3 and Table S1. (**A**) Heatmaps illustrate normalized neuronal firing (auROC) aligned to behavioral response, i.e., spout withdrawal (Time = 0 s; vertical dashed white lines). Same data as in Figures 3 and S2, but separated by groups representing task-dependent changes in tonic firing. Rows are ordered by the mean auROC preceding spout withdrawal (–0.5 to 0 s; brackets on top of heatmaps) during hit trials within each group. The same order is used across other trial types. (**B**) Phasic modulation after spout withdrawal was calculated as in Figure S2 and is illustrated as mean ± standard error across units. Mean phasic modulation (0.3 to 0.8 s) was higher in hit than false alarm and miss trials in all three groups (task-suppressed, -enhanced, -unchanged units). (**C**) Phasic modulation preceding spout withdrawal was calculated as in Figure 3. Mean phasic modulation (–0.5 to 0 s) was stronger in hit than in false alarm trials in task-suppressed and -enhanced, but not in task-unchanged units. ***p < 0.001; **p < 0.01

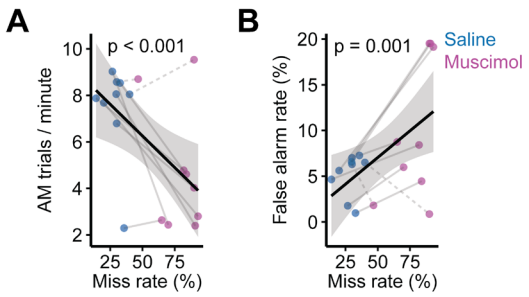

Figure S4. Slower trial completion and increased false alarm rates during OFC inactivation may be explained by the increased frequency of punishment. Related to Figure 4 and Table S1. (**A**) The number of AM trials completed per minute negatively correlates with the miss rate. (**B**) The false alarm rate positively correlates with the miss rate. Blue dots represent days when animals received saline infusions into OFC, while magenta dots represent days when animals received muscimol infusions. Gray lines connect data from the same animal. Dashed lines indicate animals that received unilateral left OFC infusions due to partially clogged cannulas.

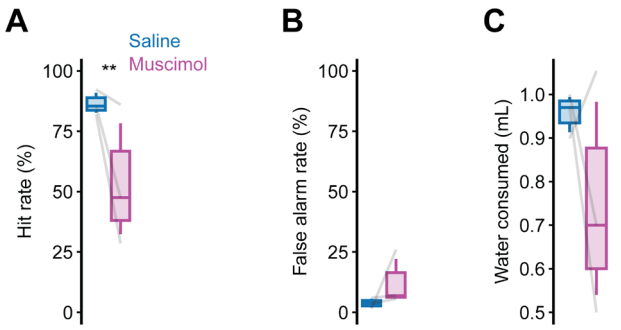

Figure S5. The behavioral effects of OFC suppression replicate in animals with chronic electrode implants in the auditory cortex. Related to Figure 5 and Table S1. OFC suppression significantly reduced behavioral hit rates (**A**) but did not significantly affect false alarm rates (**B**) or water consumed during the task (**C**). **p<0.01.

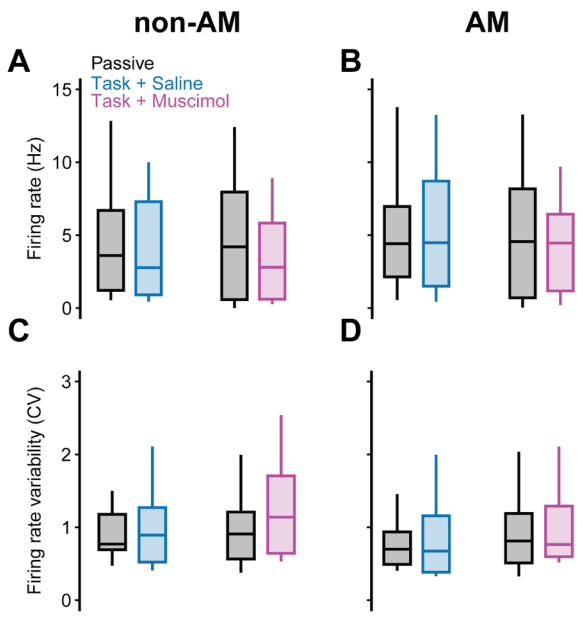

Figure S6. Effects of OFC suppression on auditory cortical firing rates and firing rate variability. Related to Figure 5 and Table S1. (**A-B**) Neither task engagement nor OFC suppression systematically affect non-AM (**A**) or AM firing rates (**B**) of auditory cortical single- and multi-units. (**C-D**) Neither task engagement nor OFC suppression systematically affect non-AM (**C**) or AM firing rate variability (**D**).

Figure	Test	Factor(s)	Statistic	P value
S2C	GLM/ANOVA	Trial type	$\chi^2_2 = 203.980$	**< 0.001**
	Bonferroni: Trial type	Hit – False alarm	$t_{1576} = 12.091$	**< 0.001**
		Hit – Miss	$t_{1576} = 12.589$	**< 0.001**
		False alarm – miss	$t_{1576} = 0.367$	>0.999
S3B	GLM/ANOVA: Task-suppressed	Trial type	$\chi^2_2 = 89.686$	**< 0.001**
	Bonferroni: Trial type	Hit – False alarm	$t_{622} = 8.188$	**< 0.001**
		Hit – Miss	$t_{622} = 8.182$	**< 0.001**
		False alarm – miss	$t_{622} = –0.104$	>0.999
	GLM/ANOVA: Task-enhanced	Trial type	$\chi^2_2 = 104.720$	**< 0.001**
	Bonferroni: Trial type	Hit – False alarm	$t_{570} = 8.984$	**< 0.001**
		Hit – Miss	$t_{570} = 8.709$	**< 0.001**
		False alarm – miss	$t_{570} = –0.347$	>0.999
	GLM/ANOVA: Task-unchanged	Trial type	$\chi^2_2 = 21.378$	**0.002**
	Bonferroni: Trial type	Hit – False alarm	$t_{370} = 3.471$	**< 0.001**
		Hit – Miss	$t_{370} = 4.371$	**< 0.001**
		False alarm – miss	$t_{370} = 0.852$	>0.999
S3C	GLM/ANOVA: Task-suppressed	Trial type	$\chi^2_1 = 20.842$	**< 0.001**
	GLM/ANOVA: Task-enhanced	Trial type	$\chi^2_1 = 31.561$	**< 0.001**
	GLM/ANOVA: Task-unchanged	Trial type	$\chi^2_1 = 2.488$	0.115
S4A	GLM/ANOVA	Miss rate	$\chi^2_1 = 15.630$	**< 0.001**
S4B	GLM/ANOVA	Miss rate	$\chi^2_1 = 10.778$	**0.001**
S5A	GLM/ANOVA	Treatment	$\chi^2_1 = 8.271$	**0.004**
S5B	GLM/ANOVA	Treatment	$\chi^2_1 = 2.715$	0.099
S5C	GLM/ANOVA	Treatment	$\chi^2_1 = 2.323$	0.127
S6A	GLM/ANOVA: Saline	Context	$\chi^2_1 = 0.678$	0.410
	GLM/ANOVA: Muscimol	Context	$\chi^2_1 = 1.900$	0.168
S6B	GLM/ANOVA: Saline	Context	$\chi^2_1 < 0.001$	0.998
	GLM/ANOVA: Muscimol	Context	$\chi^2_1 = 0.214$	0.643
S6C	GLM/ANOVA: Saline	Context	$\chi^2_1 = 0.223$	0.637
	GLM/ANOVA: Muscimol	Context	$\chi^2_1 = 0.122$	0.726
S6D	GLM/ANOVA: Saline	Context	$\chi^2_1 = 0.003$	0.959
	GLM/ANOVA: Muscimol	Context	$\chi^2_1 = 0.546$	0.460

Table S1. Statistical results. Related to Figures S2, S3, S4, S5 and S6. GLM: Generalized linear model; ANOVA: Analysis of Variance; Bolded p-values indicate statistical significance.